Photo-Sensitive RAFT-Agents for Advanced Microparticle Design

ARTICLE *in* MACROMOLECULES · AUGUST 2013

Impact Factor: 5.8 · DOI: 10.1021/ma401242g

9 AUTHORS, INCLUDING:

Astrid F. Hirschbiel
Karlsruhe Institute of Technology
6 PUBLICATIONS **35** CITATIONS
SEE PROFILE

Andrew P. Vogt
Scion
24 PUBLICATIONS **1,178** CITATIONS
SEE PROFILE

Thorsten Hofe
University of Applied Science Fresenius
20 PUBLICATIONS **143** CITATIONS
SEE PROFILE

Martina H Stenzel
University of New South Wales
279 PUBLICATIONS **11,089** CITATIONS
SEE PROFILE

Macromolecules

Article

pubs.acs.org/Macromolecules

Photo-Sensitive RAFT-Agents for Advanced Microparticle Design

Michael Kaupp,[†,⊥] Thomas Tischer,[†,⊥] Astrid F. Hirschbiel,[†,⊥] Andrew P. Vogt,[†,⊥] Udo Geckle,[‡] Vanessa Trouillet,[‡] Thorsten Hofe,[§] Martina H. Stenzel,[∥] and Christopher Barner-Kowollik*[,†,⊥]

[†]Preparative Macromolecular Chemistry, Institut für Technische Chemie und Polymerchemie, Karlsruhe Institute of Technology (KIT), Engesserstraße 18, 76128 Karlsruhe, Germany

[⊥]Institut für Biologische Grenzflächen, Karlsruhe Institute of Technology (KIT), Herrmann-von-Helmholtzplatz 1, 76344 Eggenstein-Leopoldshafen, Germany

[‡]Institute for Applied Materials (IAM-ESS), Karlsruhe Institute of Technology (KIT), Hermann-von-Helmholtz-Platz 1, 76344 Eggenstein-Leopoldshafen, Germany

[§]Polymer Standards Service GmbH, In der Dalheimer Wiese 5, 55120 Mainz, Germany

[∥]Centre for Advanced Macromolecular Design (CAMD), The University of New South Wales, Sydney NSW 2052, Australia

Supporting Information

ABSTRACT: The current contribution describes the combination of an efficient reversible deactivation radical polymerization process (reversible addition−fragmentation chain transfer (RAFT) polymerization) with a mild light-induced modular ligation technique. A novel RAFT-agent was synthesized which carries a photoactive group based on ortho-quinodimethane (photo-enol) chemistry. The novel photoreactive RAFT-agent controls the polymerization of a wide range of monomers such as styrene, *N*,*N*-dimethylacrylamide and a protected glycomonomer (2-(2′,3′,4′,6′-tetra-*O*-acetyl-*β*-D-mannosyloxy)ethyl acrylate) with dispersities between 1.07 and 1.17 (3500 g·mol^{-1} ≤ M_n ≤ 10100 g·mol^{-1}) and quantitative end-group functionalization. The photo-enol group reacts with dieneophiles under mild irradiation (λ_{max} = 320 nm) at ambient conditions − so that the RAFT-group remains intact − and without any catalyst to form block copolymers in a matter of minutes. Furthermore, the RAFT-polymers can be photografted onto porous polymeric (poly(glycidyl methacrylate)) microspheres, after a one-step prefunctionalization with maleimide moieties. The successful photografting is evidenced by scanning electron microscopy (SEM), elemental analysis (EA), X-ray photoelectron spectroscopy (XPS) and high resolution attenuated total reflectance (ATR) FT-IR microscopy, which leads to qualitative as well as quantitative grafting data. The grafting densities obtained for polystyrene are close to 0.11 chains per nm^2 (M_n = 3900 g·mol^{-1}) and for poly(*N*,*N*-dimethylacrylamide) close to 0.12 chains per nm^2 (M_n = 3500 g·mol^{-1}). To highlight the additional benefit of employing a light-induced grafting reaction, Janus microspheres were prepared with poly(*N*,*N*-dimethylacrylamide) employing a Pickering emulsion approach and illustrated via ATR-FT-IR microscopy.

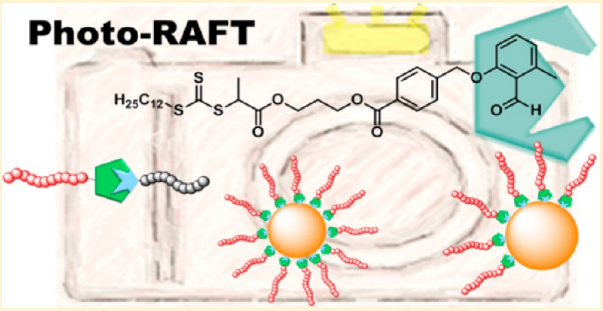

INTRODUCTION

Chemistry employing ortho-quinodimethanes[1]—termed photo-enol chemistry—has recently emerged as a mild modular ligation strategy to the toolbox of modular ligation reactions already utilized by (polymer) chemists. photo-enol chemistry has been proven as a robust yet elegant strategy to construct challenging polymer architectures[2,3] as well as for the modification of surfaces.[4] The photo-enol ligation reaction clearly fulfills the criteria of a polymeric click reaction,[5,6] however has the added benefit of affording spatial resolution, as it is driven by light. Furthermore—due to the high reactivity of the formed photo-enol diene—a vast array of dienophiles can be employed, even nonactivated dithiobenzoates of—or stemming from—reversible addition chain transfer polymerization (RAFT) agents.[7] The photo-enol ligation reaction has no need for any additional catalyst, also excluding cytotoxic copper species, which are employed for one of the most popular and widely used click reactions, i.e., as the copper catalyzed azide−alkyne cycloaddition (CuAAC).[8]

Reversible deactivation radical polymerization (RDRP) techniques provide chains with tunable lengths, low dispersities and functional end-groups. Among the most popular RDRP techniques which include nitroxide mediated polymerization,[9] atom transfer radical polymerization,[10,11] and RAFT,[12] the latter is unarguably the most versatile.[13]

The combination of easy to use RDRP techniques with modular and light-triggered conjugation techniques affords new opportunities for the modification of surfaces. Interesting

Received: June 16, 2013
Revised: July 22, 2013
Published: August 20, 2013

Scheme 1. Illustration of the Synthetic Strategy Employing the RAFT-Photo-Enol Agent DoPATPE[a]

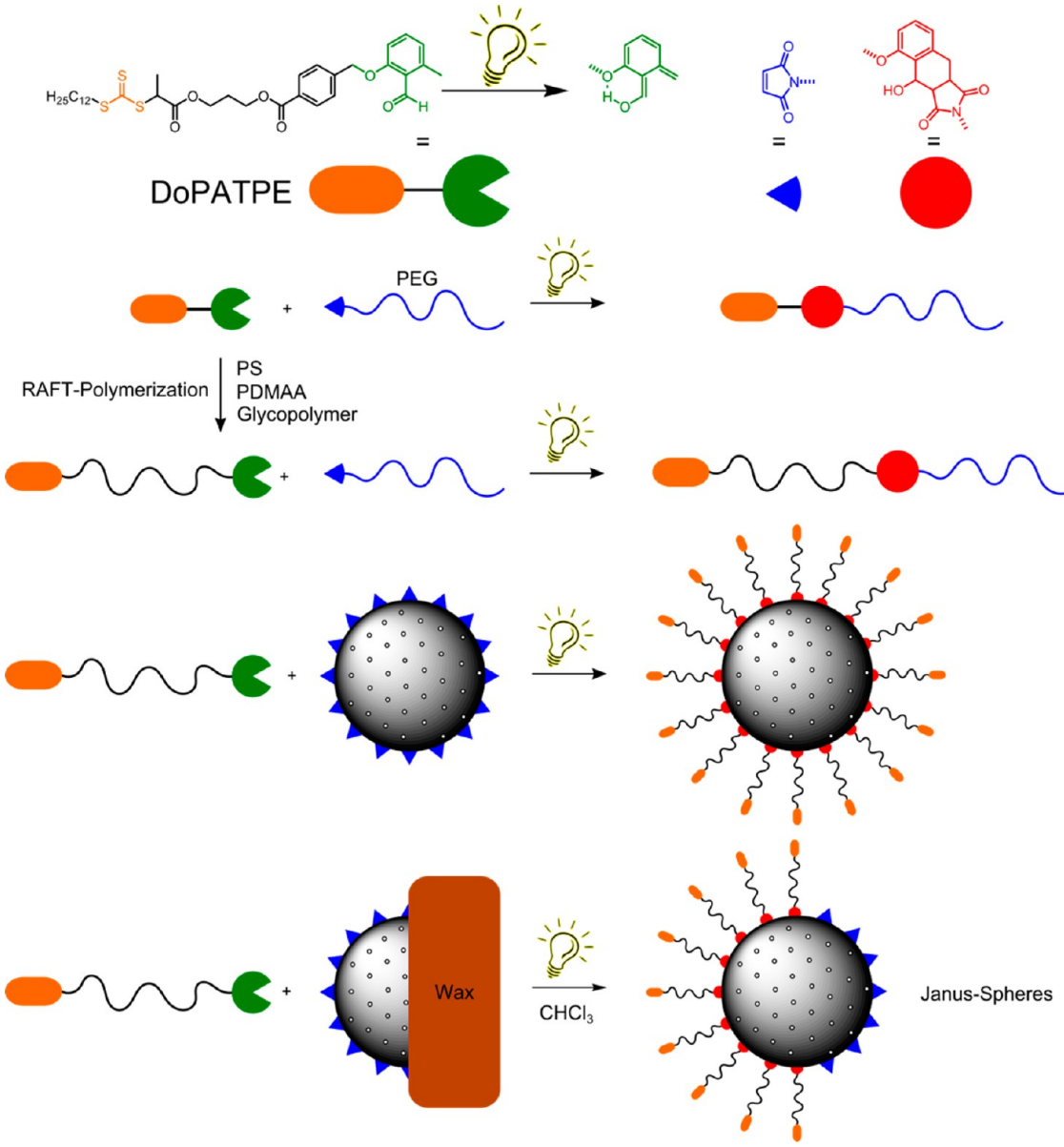

[a]The versatility and robustness of the applied approach are demonstrated as are the opportunities of employing light-triggered grafting reactions on spherical objects by synthesizing Janus particles.

substrates that can be employed in such grafting reactions are cross-linked (porous) polymeric microspheres.[14] There are many well-known pathways to synthesize cross-linked (porous) polymeric microspheres[15] and a wide range of established applications, such as in organic synthesis,[16] in chromatography[17,18] or in pharmaceuticals.[19] A major interest lies in the modification of the surface of the microspheres with polymers to introduce new/altered surface chemistries, thereby changing the microspheres' properties. There exist two basic concepts to graft polymeric chains onto microspheres.[20] "Grafting from" implies an initiating molecule is tethered to the surface of the substrate, from which the polymerization is started. Because of low steric hindrance of the propagating moiety, high grafting densities are achievable via the "grafting from" technique.[21] During a "grafting to" reaction, a reactive group on a polymeric chain reacts with a complementary group on the substrate's surface. The already attached chains may then lead to steric hindrance for further chain attachment.[22] However, the steric drawback is compensated by the modular fashion of the "grafting to" approach, which allows for a full analysis of the grafted (macro)molecule prior to attachment, which is often not feasible via the "grafting from" approach. Furthermore, it is advantageous that the chosen polymerization and grafting reaction do not influence each other, leading to a higher diversity in both the reactive end-group(s) as well as the employable monomers.

Employing highly reactive "grafting to" reactions that may even adhere to click criteria,[5,6] benefits from the high achievable grafting densities, short reaction times and nondemanding reaction conditions.[23,24] Furthermore, light-triggered reactions offer the additional benefit of spatially controlled grafting.

The current contribution describes the synthesis and application of a RAFT-agent containing a photoactive conjugation moiety as well as its use in photografting reactions.

dx.doi.org/10.1021/ma401242g | Macromolecules 2013, 46, 6858−6872

The reactivity of the functional group and the stability of the photoadduct are evidenced in model reactions. The versatility and kinetics of the approach are demonstrated via the formation of various block copolymers, including glycopolymers (a polymer in which carbohydrate moieties are incorporated).[25] In addition to the block copolymer formation, the photografting of various polymers (polystyrene, poly(*N*,*N*-dimethylacrylamide) and the glycopolymer poly(2-(2′,3′,4′,6′-tetra-*O*-acetyl-*β*-D-mannosyloxy)ethyl acrylate) onto microparticles is performed. The addition of glycopolymers onto microspheres can lead to bioactive particles.[26] To exemplify the successful spatial resolution of the photoinduced "grafting to" on the microspheres, formation of so-called Janus particles (exhibiting two different functionalized hemispheres),[27] utilizing a combination of photografting and a Pickering emulsion approach[28,29] is presented. Scheme 1 depicts a schematic overview of the synthetic strategy followed in the present study.

EXPERIMENTAL PART

Materials. 4-(2-Hydroxyethyl)-10-oxa-4-azatricyclo[5.2.1.02,6]dec-8-ene-3,5-dione,[30] maleimide-functionalized poly(ethylene glycol) (PEG-Mal),[2] and methyl 4-((2-formyl-3-methylphenoxy)methyl)-benzoic acid[4] were synthesized according to the literature. 2,2′-Azobis(2-methylpropionitrile) (AIBN) was recrystallized twice from methanol. Styrene and *N*,*N*-dimethylacrylamide (DMAA) were passed through a column of basic alumina to remove inhibitor and subsequently stored at −19 °C. Dichloromethane (DCM) was dried and stored over $CaCl_2$; *N*,*N*-dimethylformamide (DMF) was dried and stored over Na_2SO_4. Poly(glycidyl methacrylate) (PGMA) microspheres with a PGMA content of 80% and pore size of 1000 Å were synthesized by Polymer Standards Service (PSS) GmbH as described before.[31] 2-((Dodecylsulfanyl)carbonothioyl)sulfanyl propanoic acid (DoPAT) was obtained from Orica Pty Ltd., Melbourne, Australia. All other chemicals were used as supplied by the manufacturers.

Synthesis of 1-((3-Hydroxypropoxy)carbonyl)ethyl Dodecyl Carbonotrithioate (DoPATOH). DoPAT (6.00 g, 17.1 mmol, 1.00 equiv), 1,3-propanediol (3.75 mL, 3.92 g, 51.5 mmol, 3.00 equiv), and 4-dimethylaminopyridine (41.8 mg, 0.34 mmol, 0.02 equiv) were dissolved in 40 mL of dry THF. The solution was cooled to 0 °C in an ice bath and dicyclohexylcarbodiimide (4.44 g, 21.5 mmol, 1.26 equiv) dissolved in 8 mL of dry THF was added dropwise. After 1 h, the ice bath was removed and the reaction proceeded overnight at ambient temperature. The solvent was removed under reduced pressure and the residue dissolved in diethyl ether. After filtration, the organic layer was washed with 5% HCl, saturated $NaHCO_3$ solution and distilled water, dried over $MgSO_4$ and the solvent removed. The crude product was purified via column chromatography (silica gel, cyclohexane/ethyl acetate 2:1) to afford a yellow solid (6.30 g, 90%). **^{1}H NMR** ($CDCl_3$, 400 MHz), *δ*/ppm: 4.81 (q, ^3J = 7.4 Hz, 1H, $SC\underline{H}CH_3$), 4.29 (m, 2H, $HOCH_2CH_2C\underline{H}_2$), 3.69 (t, ^3J = 6.0 Hz, 2H, $HOC\underline{H}_2CH_2CH_2$), 3.34 (dt, ^3J = 7.4 Hz, ^5J = 1.3 Hz, 2H, $SC\underline{H}_2CH_2C_7H_{14}CH_2CH_2CH_3$), 1.88 (quin, ^3J = 6.0 Hz, 2H, $HOCH_2C\underline{H}_2CH_2$), 1.68 (quin, ^3J = 7.4 Hz, 2H, $SCH_2C\underline{H}_2C_7H_{14}CH_2CH_2CH_3$), 1.59 (d, ^3J = 7.4 Hz, 3H, $SCHC\underline{H}_3$), 1.39 (m, 2H, $SCH_2CH_2C_7H_{14}CH_2C\underline{H}_2CH_3$), 1.25 ($s_{br}$, 16H, $SCH_2CH_2C_7\underline{H}_{14}C\underline{H}_2CH_2CH_3$), 0.87 (t, ^3J = 6.9 Hz, 3H, $SCH_2CH_2C_7H_{14}CH_2CH_2C\underline{H}_3$). **^{13}C NMR** ($CDCl_3$, 100 MHz), *δ*/ppm: 222.1 ($S\underline{C}(S)S$), 171,5 ($SCHCH_3\underline{C}(O)O$), 62,8 ($HOCH_2CH_2\underline{C}H_2$), 59,2 ($HO\underline{C}H_2CH_2CH_2$), 47,8 ($S\underline{C}HCH_3C(O)O$), 37.3 ($S\underline{C}H_2CH_2C_7H_{14}CH_2CH_2CH_3$), 31.9 ($SCH_2CH_2C_7H_{14}\underline{C}H_2CH_2CH_3$), 31.5, ($HOCH_2\underline{C}H_2CH_2$), 29.6 (2×), 29.5, 29.4, 29.3, 29.1, 28.9, 27.9 (8C, $SCH_2\underline{C}H_2\underline{C}_7H_{14}CH_2CH_2CH_3$), 22.7 ($SCH_2CH_2C_7H_{14}CH_2\underline{C}H_2CH_3$), 16.8 ($S\underline{C}HCH_3C(O)O$), 14.1 ($SCH_2CH_2C_7H_{14}CH_2CH_2\underline{C}H_3$). **MS**: (ESI) *m*/*z* calculated for $C_{19}H_{36}O_3S_3$ [M + Na]$^+$, 431.17; found, 431.16.

Synthesis of DoPAT-Photo-Enol (DoPATPE). DoPATOH (1.50 g, 3.67 mmol, 1.00 equiv), 4-((2-formyl-3-methylphenoxy)methyl)-benzoic acid (1.14 g, 4.22 mmol, 1.15 equiv) and 4-dimethylaminopyridine (116 mg, 0.95 mmol, 0.26 equiv) were dissolved in dry DMF. Dicyclohexylcarbodiimide (1.16 g, 5.65 mmol, 1.35 equiv) dissolved in dry DMF was added dropwise. The reaction was covered with aluminum foil to protect it from ambient light. The reaction proceeded for 46 h at ambient temperature; subsequently, 100 mL DCM was added and the organic layer was washed with 5% HCl, saturated $NaHCO_3$ solution and distilled water, dried over Na_2SO_4 and the solvent removed. The crude product was purified via column chromatography (silica gel, cyclohexane/ethyl acetate 2:1) to give a yellow solid (1.48 g, 61%). **^{1}H NMR** ($CDCl_3$, 300 MHz), *δ*/ppm: 10.75 (s, 1H, C$\underline{H}$O), 8.06 (d, ^3J = 8.3 Hz, 2H, paraAr*H*), 7.50 (d, ^3J = 8.4 Hz, 2H, paraAr*H*), 7.36 (t, ^3J = 8.0 Hz, 2H, Ar*H*), 6.85 (m, 2H, Ar*H*), 5.24 (s, 2H, ArC$\underline{H}_2$O), 4.81 (q, ^3J = 7.4 Hz, 1H, $SC\underline{H}CH_3$), 4.42 (t, ^3J = 6.2 Hz, 2H, $ArC(O)OCH_2CH_2C\underline{H}_2$), 4.33 (m, 2H, $ArC(O)OC\underline{H}_2CH_2CH_2$), 3.35 (dt, ^3J = 7.4 Hz, ^5J = 1.0 Hz, 2H, $SC\underline{H}_2CH_2C_7H_{14}CH_2CH_2CH_3$), 2.61 (s, 3H, $ArC\underline{H}_3$), 2.15 (quin, ^3J = 6.2 Hz, 2H, $ArC(O)OCH_2C\underline{H}_2CH_2$), 1.68 (quin, ^3J = 7.4 Hz, 2H, $SCH_2C\underline{H}_2C_7H_{14}CH_2CH_2CH_3$), 1.61 (d, ^3J = 7.4 Hz, 3H, $SCHC\underline{H}_3$), 1.27 (s_{br}, 18H, $SCH_2CH_2C_7\underline{H}_{14}C\underline{H}_2C\underline{H}_2CH_3$), 0.89 (t, ^3J = 6.9 Hz, 3H, $SCH_2CH_2C_7H_{14}CH_2CH_2C\underline{H}_3$). **^{13}C NMR** ($CDCl_3$, 75 MHz), *δ*/ppm: 222.0 ($S\underline{C}(S)S$), 191.9 ($\underline{C}HO$), 171,1 ($ArC(O)OCH_2CH_2CH_2\underline{C}(O)O$), 165.9 ($ArC(O)OCH_2CH_2CH_2C(O)O$), 161.8 (Ar), 142.3 (paraAr), 141.4 (Ar), 134.4 (Ar) 130.0, 129.9, 126.8 (paraAr), 124.7, 123.6, 110.3 (Ar), 69.9 ($ArC\underline{H}_2O$), 62.4 ($ArC(O)OCH_2CH_2\underline{C}H_2C(O)O$), 61.4 ($ArC(O)O\underline{C}H_2CH_2CH_2C(O)O$), 47.8 ($S\underline{C}HCH_3$), 37.2 $S\underline{C}H_2CH_2C_7H_{14}CH_2CH_2CH_3$), 31.9 ($SCH_2CH_2C_7H_{14}\underline{C}H_2CH_2CH_3$), 29.6 (2×), 29.5, 29.4, 29.3, 29.0, 28.9, 27.9, (8C, $SCH_2\underline{C}H_2\underline{C}_7H_{14}CH_2CH_2CH_3$), 27.8 ($ArC(O)OCH_2\underline{C}H_2CH_2C(O)O$), 22.6 ($SCH_2CH_2C_7H_{14}CH_2\underline{C}H_2CH_3$), 21.4 ($Ar\underline{C}H_3$), 16.7 ($SCH\underline{C}H_3C(O)O$), 14.1 ($SCH_2CH_2C_7H_{14}CH_2CH_2\underline{C}H_3$). **MS**: (ESI) *m*/*z* calculated for $C_{35}H_{48}O_6S_3$ [M + Na]$^+$, 683.25; found, 683.32.

Synthesis of 2-(2′,3′,4′,6′-Tetra-*O*-acetyl-*β*-D-mannosyloxy)-ethyl Acrylate (AcManEA). *Peracetylation of Mannose.* Mannose (5.00 g, 27.7 mmol, 1.00 equiv) was suspended in acetic anhydride (26.2 mL, 28.3 g, 277 mmol, 10.0 equiv). The mixture was cooled to 0 °C with an ice bath and two drops of sulfuric acid were added, which led to the formation of a clear solution. After 30 min, the ice bath was removed and the reaction proceeded at ambient temperature overnight. 100 mL of water was added and the solution was extracted three times with ethyl acetate. The organic phase was alternately washed with saturated $NaHCO_3$ solution and distilled water until the water was neutral after the washing procedure. The organic phase was dried over $MgSO_4$ and the solvent removed under reduced pressure to give a colorless waxy solid (8.89 g, 82%). **^{1}H NMR** ($CDCl_3$, 400 MHz), *δ*/ppm: 6.07 (s, 1H, anomeric C), 5.31, 4.17 (2 multiplets, each 3H, sugar moiety), 2.16, 2.15, 2.08, 2.04, 1.99 (5 s, each 3H, acetyl-groups). **^{13}C NMR** ($CDCl_3$, 100 MHz), *δ*/ppm: 170.6, 170.0, 169.7, 169.5, 168.0 (5C, $H_3CC(O)O$), 90.5 (anomeric C), 70.5, 68.7, 68.3, 65.5, 62.1 (5C, sugar moiety), 20.8, 20.7, 20.7 20.6, 20.6 (5C, $H_3\underline{C}C(O)O$). **MS**: (ESI) *m*/*z* calculated for $C_{16}H_{22}O_{11}$ [M + Na]$^+$, 413.11; found, 413.12.

Acetalization with 2-Hydroxyethyl Acrylate. The synthesis was carried out based on a modified literature method.[32]

β-D-Mannose pentaacetate (1.98 g, 5.07 mmol, 1.00 equiv) was dissolved in dry DCM and 2-hydroxyethyl acrylate (700 *μ*L, 706 mg, 6.08 mmol, 1.20 equiv) was added. The mixture was cooled to −10 °C with an ice/salt-bath and $BF_3{\cdot}OEt_2$ (3.60 g, 25.4 mmol, 5.00 equiv) was added dropwise. The reaction was allowed to reach ambient temperature and was stirred overnight. After addition of 10 mL of water, the mixture was extracted with DCM and the organic phase washed with water, saturated $NaHCO_3$ solution and again water. After drying over Na_2SO_4, the solvent was removed under reduced pressure. The crude product was purified via column chromatography (silica gel, cyclohexane/ethyl acetate 1:3) to afford a colorless liquid (1.73 g, 76%), which was stored at −19 °C and used rapidly to prevent autopolymerization. **^{1}H NMR** ($CDCl_3$, 400 MHz), *δ*/ppm: 6.43 (d, ^3J = 17.3 Hz, 1H, vinylic H), 6.13 (m, 1H, vinylic H), 5.86 (d, ^3J = 10.4 Hz, 1H, vinylic H), 5.28 (m, 3H, sugar moiety), 4.86 (s, 1H, sugar moiety), 4.14 (m, 6H, sugar and ethyl moiety), 3.83 (m, 2H, ethyl

dx.doi.org/10.1021/ma401242g | Macromolecules 2013, 46, 6858−6872

moiety), 2.14, 2.08, 2.03, 1,98 (4 s, each 3H, acetyl groups). **^{13}C NMR** ($CDCl_3$, 100 MHz), δ/ppm: 170.6, 170.0, 169.8, 169.7 (4C, $H_3C\underline{C}(O)O$), 165.8 ($H_2CCH\underline{C}(O)O$), 131.3 ($H_2\underline{C}CHC(O)O$), 128.0 ($H_2C\underline{C}HC(O)O$), 97.6 (anomeric C), 69.4, 68.9, 68.6, 6.1, 66.0, 62.9, 62.4 (7C, sugar and ethyl moiety), 20.8, 20.7 20.6, 20.6 (4C, $H_3\underline{C}C(O)O$). **MS**: (ESI) m/z calculated for $C_{19}H_{26}O_{12}$ $[M + Na]^+$, 469.13; found, 469.20.

RAFT-Polymerizations. *Synthesis of Polystyrene (PS).* A solution of AIBN (3.8 mg, 0.023 mmol, 0.10 equiv) and DoPATPE (153 mg, 0.23 mmol, 1.00 equiv) in styrene (2.40 g, 23.0 mmol, 100 equiv) was deoxygenated with three consecutive freeze−pump−thaw cycles. The reaction was placed into a preheated oil-bath at 60 °C for 14 h. The reaction was stopped by cooling in an ice-bath and exposing the reaction mixture to oxygen. The polymer was isolated by 2-fold precipitation in cold methanol and subsequent drying under vacuum to afford 596 mg of a slightly yellow powder. M_n = 3900 g·mol^{-1}, $Đ$ = 1.07 (GPC in THF, polystyrene calibration).

Synthesis of Poly(N,N-dimethylacrylamide) (PDMAA). A solution of AIBN (9.6 mg, 0.058 mmol, 0.2 equiv), DoPATPE (194.0 mg, 0.29 mmol, 1.00 equiv) and DMAA (1.46 g, 14.7 mmol, 50 equiv) in DMF (7.5 mL) was deoxygenated with three consecutive freeze−pump−thaw cycles. The reaction was placed into a preheated oil-bath at 60 °C for 3 h. The reaction was stopped by cooling in an ice-bath and exposing the reaction mixture to oxygen. The polymer was isolated by dialyzing the reaction mixture against distilled water (utilizing a SpectraPor3 membrane (MWCO = 1000 Da)) and subsequent freeze-drying to give 597 mg of a yellow solid. M_n = 3500 g·mol^{-1}, $Đ$ = 1.11 (GPC in dimethylacetamide (DMAc), polystyrene calibration).

Synthesis of Poly(2-(2′,3′,4′,6′-tetra-O-acetyl-β-D-mannosyloxy)-ethyl acrylate) (PAcManEA). A solution of AIBN (0.64 mg, 0.004 mmol, 0.10 equiv), DoPATPE (25.6 mg, 0.038 mmol, 1.00 equiv) and AcManEA (1.73 g, 3.88 mmol, 100 equiv) in DMAc (8.0 mL) was deoxygenated with three consecutive freeze−pump−thaw cycles. The reaction was placed into a preheated oil-bath at 60 °C for 3 h. The reaction was stopped by cooling in an ice-bath and exposing the reaction mixture to oxygen. The polymer was isolated by precipitation in cold diethyl ether and dried under vacuum to give 414 mg of a slightly yellow, waxy solid. M_n = 5700 g·mol^{-1}, $Đ$ = 1.17 (GPC in THF, polystyrene calibration); M_n = 10100 g·mol^{-1}, $Đ$ = 1.14 (GPC in DMAc, polystyrene calibration). The block copolymer formation showed that the results from the GPC in DMAc are accurate, as for a successful reaction the stoichiometry has to be precise.

Maleimide-Functionalization of PGMA Microspheres. PGMA microspheres (1.24 g, 7.70 mmol, 1.00 equiv of epoxy groups) and 4-(2-hydroxyethyl)-10-oxa-4-azatricyclo[5.2.1.02,6]dec-8-ene-3,5-dione (1.61 g, 7.70 mol, 1.00 equiv) were mixed in 1,4-dioxane (100 mL) and BF_3·OEt_2 (1.00 mL, 1.13 g, 7.96 mmol, 1.03 equiv) was added. The reaction was shaken at 60 °C overnight to attach the protected maleimide to the microspheres and subsequently heated for 7 h to 95 °C for the deprotection of the maleimide. The microspheres were filtered off and washed with 100 mL of distilled water, acetone, THF, DCM, and acetone and subsequently dried for 2 days at 50 °C under vacuum to afford 1.36 g of an off-white powder.

Photo-Reactions. *Model Reaction.* PEG−maleimide (M_n approximately 1300 g·mol^{-1}, 40.0 mg, 0.031 mmol, 1.00 equiv) and DoPATPE (22.6 mg, 0.034 mmol, 1.10 equiv) were dissolved in acetonitrile. Equal volumes of the solution were aliquoted into vials (Pyrex, diameter 20 mm), which were crimped airtight with styrene/butadiene rubber seals; each sample was deoxygenated by purging with nitrogen for 20 min. The vials were irradiated for a predetermined time by rotating around a compact low-pressure fluorescent lamp (Arimed B6, Cosmedico GmbH, Stuttgart, Germany, 36 W) emitting at 320 nm ±30 nm) at a distance of 40−50 mm in a custom built photoreactor (see Supporting Information, Figure S 9, for details). After irradiation, the solvent was removed under reduced pressure. A particularly suitable solvent for the photoreactions is acetonitrile, which was thus employed throughout the current study.

Block Copolymer Formation. PEG−maleimide (M_n approximately 2300 g·mol^{-1}) and the RAFT-based polymer (PDMAA, PAcManEA) were dissolved in 8 mL acetonitrile in the case of PDMAA or in 8 mL of a 1:1 mixture of acetonitrile and DCM in the case of PAcManEA, respectively. The mixture was deoxygenated via three consecutive freeze−pump−thaw cycles. In an argon glovebox, the solution was aliquoted into 8 vials (Pyrex, diameter 20 mm), which were crimped airtight with styrene/butadiene rubber seals. The vials were subsequently irradiated under the conditions described above. After irradiation, the solvent was removed under reduced pressure and the residue analyzed via GPC.

For the control reaction, the RAFT-polymer was treated analogous without any addition of PEG−maleimide.

Grafting Reactions and Control Reaction on Microspheres. The microspheres and DoPATPE or RAFT-polymer, respectively, were mixed in equimolar amounts of their functional groups in DCM (4 mL in the case of DoPATPE, 5 mL in the case of the RAFT- polymers PS, PDMAA, PAcManEA) (refer to Table 1 for details). The mixture was deoxygenated with three consecutive freeze−pump−thaw cycles. The Schlenk-tubes were subsequently irradiated for 30 min under the conditions described above. The microspheres were filtered off and washed three times with DCM and dried for two days at 50 °C under vacuum prior to analysis.

Table 1. Details and Weigh-ins of Control and Grafting Reactions on Microspheres (MS)

type of MS (amount)	grafted molecule (amount)
GMA (83.3 mg, 0.45 mmol epoxide)	DoPATPE (80.1 mg, 0.12 mmol photo-enol)
Mal (80.4 mg, 0.12 mmol maleimide)	DoPATPE (81.7 mg, 0.12 mmol photo-enol)
Mal (41.6 mg, 47 μmol maleimide)	PS (190 mg, 49 μmol photo-enol)
Mal (26.6 mg, 30 μmol maleimide)	PAcManEA (190 mg, 19 μmol photo-enol)
Mal (59.7 mg, 67 μmol maleimide)	PDMAA (85.2 mg, 33.4 μmol photo-enol)

Synthesis of Janus Particles. Pickering Emulsion with Paraffin Wax. Paraffin wax (melting point 58−60 °C, 1.00 g) and maleimide-functionalized microspheres (100 mg) were heated in an oil bath to 75 °C until the wax was melted. Water (10 mL) was added and the emulsion vigorously stirred at that temperature for 1 h and subsequently for 2 h without heating to reach ambient temperature. The wax spheres were filtered off, washed extensively with distilled water and dried under vacuum.

Photo-Grafting of PDMAA. Wax spheres (diameter approximately 5 mm)—with maleimide-functionalized microspheres embedded on their surface (approximately 7 μm, half covered by wax) (246 mg)—and PDMAA (36.5 mg) were mixed in methanol (5 mL) in a Schlenk-tube. The mixture was deoxygenated via three consecutive freeze−pump−thaw cycles. The Schlenk-tube was subsequently irradiated for 30 min under the conditions described above. The wax spheres were filtered off and subsequently dissolved in $CHCl_3$. The microspheres were filtered off, washed with $CHCl_3$, twice with DCM and methanol and dried under vacuum.

Analysis. *Gel Permeation Chromatography (GPC).* GPC measurements were performed on a Polymer Laboratories PL-GPC 50 Plus Integrated System, comprising an autosampler, a PLgel 5 mm bead-size guard column (50 × 7.5 mm) followed by three PLgel 5 mm MixedC columns (300 × 7.5 mm) and a differential refractive index detector using THF at 35 °C or *N,N*-dimethylacetamide (DMAc) containing 0.3% LiBr at 50 °C as the eluent with a flow rate of 1 mL·min^{-1}. The GPC system was calibrated using linear polystyrene standards ranging from 160 to 6 × 10^6 g·mol^{-1}. All GPC calculations were carried out relative to polystyrene calibration (Mark−Houwink parameters K = 14.1 × 10^{-5} dL·g^{-1}, α = 0.70).[33]

Scanning Electron Microscopy (SEM). The morphology of the microspheres was studied on a Zeiss Supra 55. The samples were sputter-coated with 30 nm of gold before the measurement.

Electrospray Ionization-Mass Spectrometry (ESI-MS). Spectra were recorded on an LXQ mass spectrometer (Thermo-Fisher

Scheme 2. Synthesis and Structural Information of the Photo-Enol RAFT-Agent DoPATPE

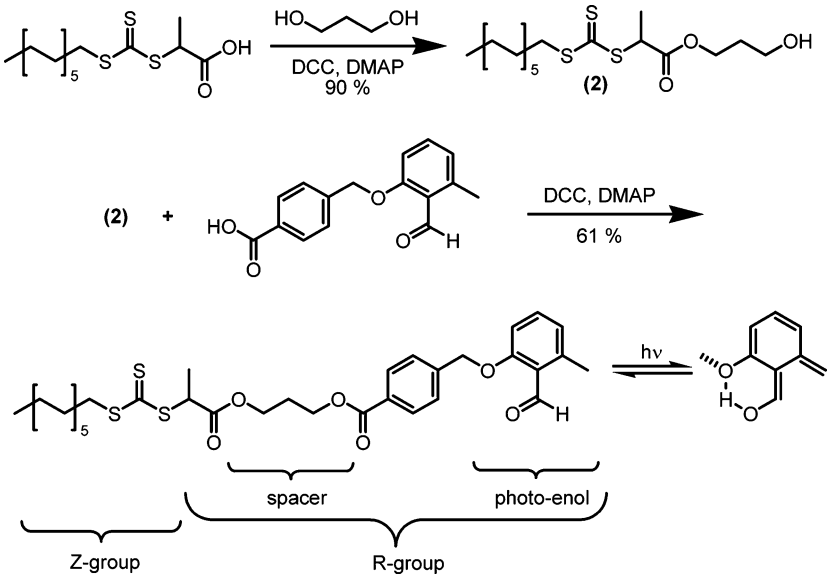

Scientific, San Jose, CA) equipped with an atmospheric pressure ionization source operating in the nebulizer assisted electrospray mode. The instrument was calibrated in the m/z range 195−1822 using a standard containing caffeine, Met-Arg-Phe-Ala acetate (MRFA) and a mixture of fluorinated phosphazenes (Ultramark 1621) (all from Aldrich). A constant spray voltage of 6 kV was used and nitrogen at a dimensionless sweep gas flow rate of 2 (approximately 3 L·min^{-1}) and a dimensionless sheath gas flow rate of 5 (approximately 0.5 L·min^{-1}) were applied. The capillary voltage, the tube lens offset voltage and the capillary temperature were set to 10 V, 70 V, and 300 °C respectively. The samples were dissolved with a concentration of 0.1 mg·mL^{-1} in a mixture of THF and MeOH (3:2) containing 100 μmol of sodium triflate and infused with a flow of 10 μL·min^{-1}.

Nuclear Magnetic Resonance (NMR) Spectroscopy. NMR measurements were conducted on a Bruker Ascend 400 or a Bruker Avance III spectrometer at 400 or 300 MHz, respectively, for hydrogen nuclei. Samples were dissolved in $CDCl_3$ or DMSO-d_6 using residual solvent peaks for shift correction.

X-ray Photoelectron Spectroscopy (XPS). XPS investigations were performed on a K-Alpha spectrometer (Thermo Fisher Scientific, East Grinstead, UK) using a microfocused, monochromated Al Kα X-ray source (400 μm spot size). The kinetic energy of the electrons was measured by a 180° hemispherical energy analyzer operated in the constant analyzer energy mode (CAE) at 50 eV pass energy for elemental spectra. The photoelectrons were detected at an emission angle of 0° with respect to the normal of the sample surface. The K-Alpha charge compensation system was employed during analysis, using electrons of 8 eV energy and low-energy argon ions to prevent any localized charge build-up.

Data acquisition and processing using the Thermo Avantage software is described elsewhere.[34] The spectra were fitted with one or more Voigt profiles (BE uncertainty: (±0.2 eV)). The analyzer transmission function, Scofield[35] sensitivity factors, and effective attenuation lengths (EALs) for photoelectrons were applied for quantification. EALs were calculated using the standard TPP-2 M formalism.[36] All spectra were referenced to the C 1s peak of hydrocarbon at 285.0 eV binding energy, controlled by means of the well-known photoelectron peaks of metallic Cu, Ag, and Au, respectively.

Elemental Analysis (EA). The elemental composition of the microsphere samples was analyzed using an automatic elemental analyzer Flash EA1112 from Thermo Scientific, which was equipped with a MAS 200R auto sampler. More details can be found in the Supporting Information of ref 37.

High Resolution Attenuated Total Reflectance (ATR) FT-IR Microscopy Imaging. Infrared measurements were performed using a Bruker FT-IR microscope HYPERION 3000 coupled to a research spectrometer VERTEX 80. The HYPERION 3000 microscope is equipped with two types of detectors: a single element MCT-detector (Mercury Cadmium Telluride) for the conventional mapping approach and a multielement FPA-detector (focal plane array) for imaging. The FPA-detector was used for the laterally resolved measurements. The multielement FPA-detector consists of 64 × 64 elements. This allows for the simultaneous acquisition of 4096 spectra covering a sample area of 32 × 32 mm (for ATR detection). With the FPA-detector in combination with the 20× Germanium ATR-lens, a lateral pixel resolution of 0.25 μm^2 is achieved, with the optical resolution depending on the employed wavelength (1000 cm^{-1} to ∼1 μm lateral resolution). For postprocessing, baseline correction and atmospheric compensation were employed.

RESULTS AND DISCUSSION

Photo-RAFT-Agent Design. The novel molecule combining a RAFT and photo-enol moiety is based on a widely used trithiocarbonate (DoPAT) and a well-known, very reactive ortho-quinodimethane connected by a small spacer to prevent any interactions between the two functional groups. The synthesis consists of two simple Steglich-esterifications[38] (see Scheme 2). In principle, all basic RAFT-agent groups (dithioesters, dithiocarbamates, and xanthates) could have been employed, yet trithiocarbonates do not undergo a cycloaddition with the highly reactive diene formed by the photo-enol under UV-irradiation[7] and have proven to be stable under the applied reaction conditions (close to 320 nm irradiation).[39,40] Nevertheless, the photo-enol group was attached to the so-called R-group, so that even if the trithiocarbonate degrades during the photoreaction, the polymer does not lose the photoactive group. In addition, attaching the photo-enol to the above-mentioned classes of RAFT-agents could in the future be utilized for the formation of cyclic polymers, based on a reaction between the α- and ω-end of a polymeric chain, or for the combination with the RAFT hetero-Diels−Alder approach.[41]

Model Reaction and Stability Assay. To assess if the trithiocarbonate is influencing the reactivity of the photo-enol and/or stability of the product several test reactions were

dx.doi.org/10.1021/ma401242g | Macromolecules 2013, 46, 6858−6872

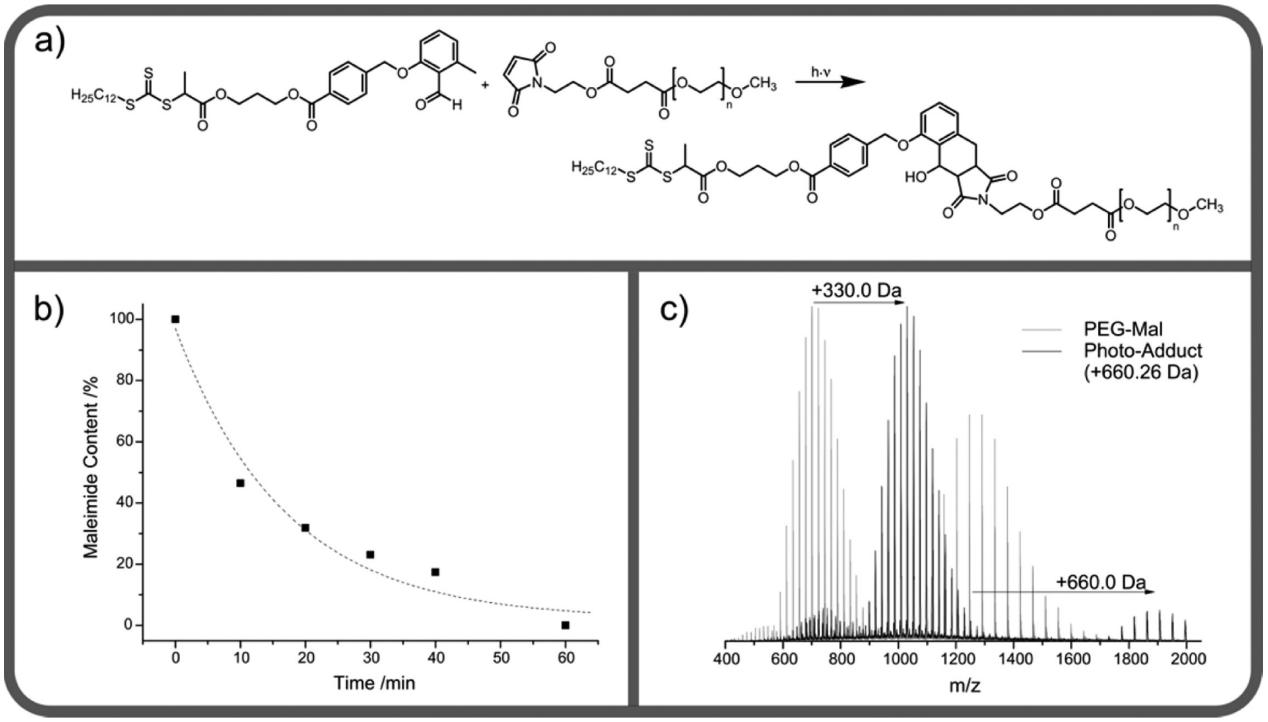

Figure 1. Model reaction between DoPATPE and a maleimide-functionalized poly(ethylene glycol) (PEG-Mal): (a) Chemical reaction scheme; (b) Kinetic investigation; Comparison of the NMR integrals of the maleimide double bond (6.72 ppm) and the methyl ether (3.36 ppm); after 60 min no maleimide can be observed. The dashed line is an exponential decay fit, but should be considered as a guide to the eye only; (c) ESI-MS comparison of the starting material (PEG-Mal) and the photoadduct after 60 min. The shift of the peaks matches the mass of DoPATPE (660 Da for single charged peaks, 330 Da for double charged peaks). No other species are observed, underlining full conversion and stability of the photoadduct. For peak assignments and more detailed mass spectra refer to the Supporting Information (Figure S 13–15 and Table S 1).

conducted. Irradiation of the dissolved DoPATPE for 30 min does not lead to a degradation as no change in the NMR nor in the mass spectrum is observable (See Figure S 10 for a comparison of the NMR spectra before and after irradiation). For an initial reactivity test a suitable counterpart was needed. A maleimide-functionalized poly(ethylene glycol) (PEG-Mal) with a molecular weight of around 1300 g·mol^{-1} was chosen, as it has shown before to be a reactive dienophile in various Diels–Alder reactions. Additionally, choosing PEG-Mal of 1300 g·mol^{-1} allows for the products and side products to be readily analyzed via ESI-MS (Figure 1).

For a kinetic study of the photoaddition, a solution containing DoPATPE and PEG-Mal in acetonitrile was degassed and separated into vials, which were irradiated for 10, 20, 30, 40, and 60 min. To assess the conversion, the samples were analyzed via NMR and the integrals of the maleimide double bond (at 6.72 ppm) compared to the integral of the methyl ether (at 3.36 ppm) (Figure 1b). Already after 10 min, 53% conversion is reached and after 60 min there is no more maleimide resonance observable in the NMR-spectrum (see Figure S 12). The dashed line is an exponential decay fit, yet should only be considered as a guide to the eye. Results discussed later indicate that for reactions employing end-functionalized polymers and lower concentrations irradiation times of 30 min or even less are sufficient to achieve full conversion. In addition to analysis via NMR, the reaction was analyzed via ESI-MS (Figure 1 c and Figure S 13–15). The spectrum after 60 min does not show any left-over starting material. A clear shift of the main peak by 660 Da for single charged ions and 330 Da for double charged ions, respectively, underpins the addition of DoPATPE (exact mass: 660.26 Da). Some smaller signals stem from triple charged ions. No other species can be observed, proving again the stability of the product. Furthermore, the increase in mass (and therefore hydrodynamic volume) can be observed via GPC analysis (see Figure S 16). Once more, no leftover PEG-Mal can be observed via GPC, and the signal of the product block is clearly shifted to a higher retention time with no shoulders or tailing which would indicate side products.

RAFT-Polymerization. The novel photoreactive RAFT-agent was tested in polymerizations of styrene, dimethylacrylamide and a protected glycomonomer (AcManEA) to demonstrate its versatility in mediating a wide range of polymerizations. The polymerization reactions were conducted in bulk, in the case of styrene, as well as in solution. An even broader study employing additional monomers including detailed kinetic data is currently conducted in our laboratory and will be published elsewhere.[42] The resulting polymers were analyzed via GPC, NMR and ESI-MS. The GPC traces show narrow dispersities, all well below 1.2 (see Figures S 18, S 21, S 24, and S 25). Only in the case of PDMAA, a small shoulder at higher retention times can be found, probably due to transfer to polymer reactions. In the ^{1}H NMR spectra, all resonances associated with the photo-enol and RAFT-end-groups can be observed (provided that they are not covered by signals from the polymeric chain) (see Figure S 17, S 20, and S 23) which allows to deduce the (number-averaged) molecular weight. The molecular weights determined via GPC and NMR are in excellent agreement for the PS sample, as they both yield 3900 g·mol^{-1}. In the case of PDMAA, the results are similar, yet they differ substantially for PAcManEA (see Experimental Part). In both of these cases, the discrepancy can be explained, as no

dx.doi.org/10.1021/ma401242g | Macromolecules 2013, 46, 6858–6872

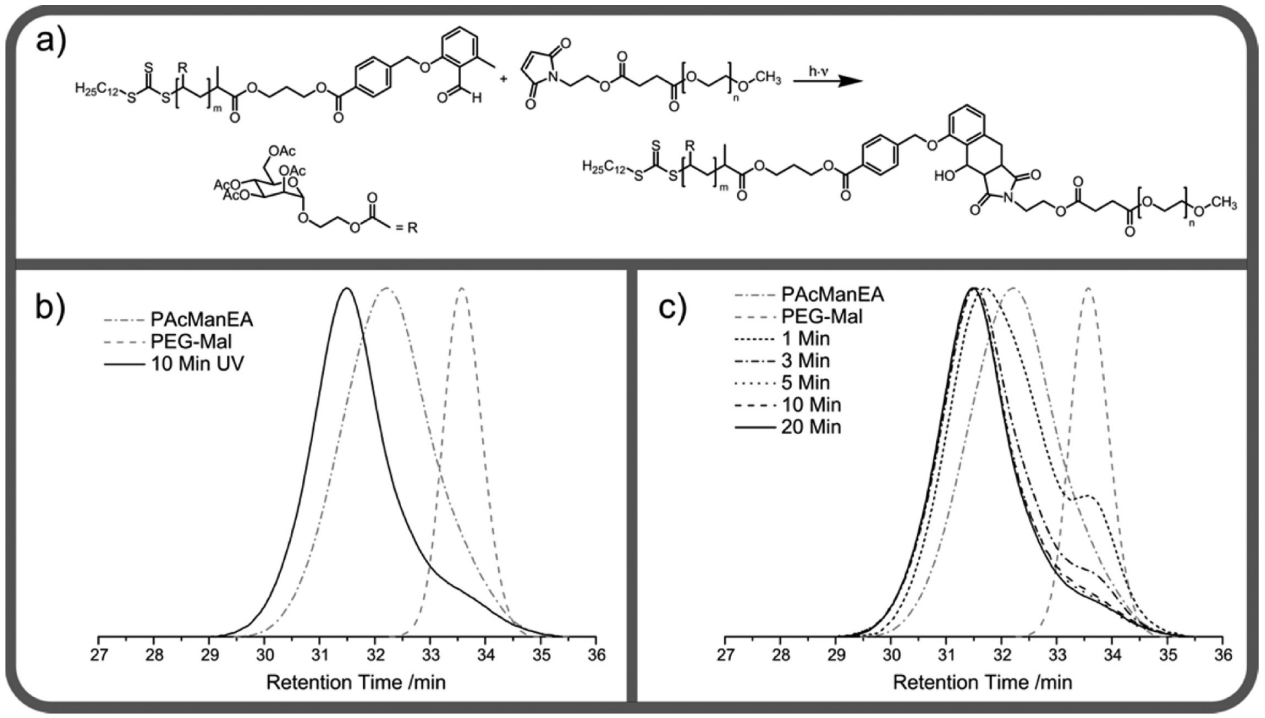

Figure 2. Light-triggered block copolymer formation between PAcManEA and PEG-Mal: (a) chemical reaction scheme; (b) comparison of the GPC traces in THF of the starting materials and the block copolymer formed after 10 min irradiation, where a clear shift to higher retention times underpins the successful photoinduced formation of the PAcManEA-*b*-PEG block copolymer; (c) kinetic investigation. The main reaction is completed after 5 min; no change can be observed after 20 min.

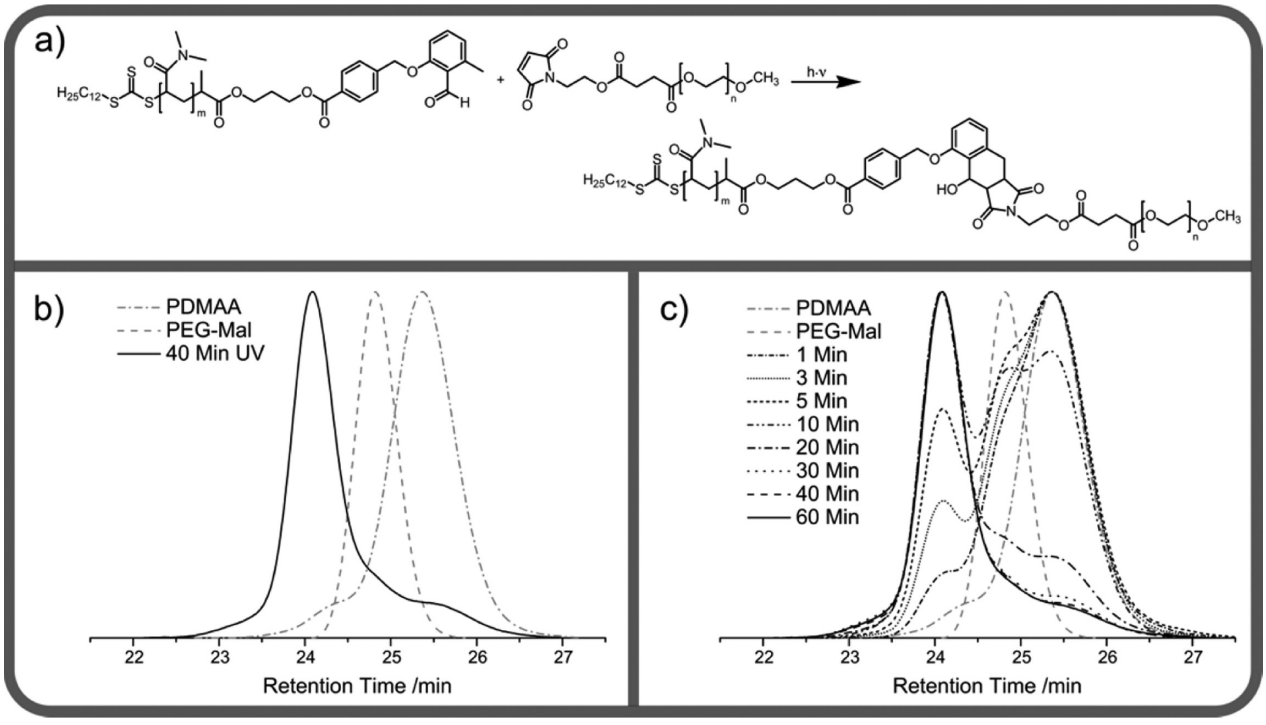

Figure 3. Light-triggered block copolymer formation between PDMAA and PEG-Mal: (a) chemical reaction scheme; (b) comparison of the GPC traces in DMAc of the starting materials and the block copolymer formed after 40 min irradiation, where a clear shift to higher retention times underpins the successful formation of the PDMAA-*b*-PEG block copolymer; (c) kinetic investigation. The main reaction is completed after 30 min; no change can be observed after 40 min.

MHKS parameters are available for the given analytical conditions, implying they have to be interpreted as PS samples. Furthermore, in the case of PAcManEA, it is difficult to integrate the signals in the NMR spectrum, as the side group signals are very broad and the ^{1}H resonances of the lateral chain overlap with several resonances of the end-groups. An in-depth

dx.doi.org/10.1021/ma401242g | *Macromolecules* 2013, 46, 6858−6872

analysis of the PS and PDMAA samples via ESI-MS reveals that there exists only one species of polymeric chains in the spectrum, namely chains with the end-groups stemming from the fragments of the RAFT-agent (labeled P_{RZ} in Figures S 19 and S 22). No signals from termination events or chains initiated by the radical initiator can be identified. Since there is a potential bias of the ionization with molecular weight, no information regarding the length of the polymer can or should be obtained from these measurements. The relatively high molecular weight of the PAcManEA (M_n = 10100 g·mol^{-1}) did not allow for an ESI-MS analysis, yet the results from the block copolymer formation (see below) suggest that the molecular weights derived via DMAc SEC are accurate as for a successful reaction the stoichiometry has to be precise.

All of the analytical results of the polymers demonstrate that the novel RAFT-agent is capable of inducing a polymerization with living characteristics without disturbance by or degradation of the photo-enol group.

Block Copolymer Formation. To investigate the reactivity of the photo-enol group—when installed at a polymer chain end via the RAFT-process—it was ascertained if these polymers can undergo photoinduced block copolymer formation with a suitable counterpart. Similar to the above-described model reaction, a maleimide-functionalized poly(ethylene glycol) (PEG-Mal) was employed. The synthesis of this PEG-Mal is identical to the one noted above, with the exception that the starting material featured double the molecular weight (2000 g·mol^{-1}, resulting in a molecular mass of the PEG-Mal of 2300 g·mol^{-1}) to obtain a larger shift in the GPC-trace for a successful reaction. The reaction itself is straightforward: A 1:1 mixture of the photo-enol RAFT-polymer and the PEG-Mal in a suitable solvent is degassed and aliquoted into several Pyrex glass vials. The vials are irradiated for a predetermined time and analyzed (after removal of the solvent) via GPC. A successful reaction is indicated by a shift of the signal to lower retention times (implying a higher hydrodynamic volume due to the higher molecular weight) and a disappearance of traces associated with the starting material.[43,44]

Since the exact molecular weight of the PAcManEA was difficult to determine, several weigh-ins had to be conducted, and analysis after the reaction indicated which reaction partner was added in excess. Finally, an equimolar ratio was reached and the results of the successful reaction are shown in Figure 2. The peak is clearly shifted to lower retention times indicating a successful block copolymer formation. A small shoulder in the GPC trace at higher retention times is visible, indicating left over PEG-Mal. The left over material is not caused by a nonequimolar reactant ratio, as several reactions were conducted and for the reactions with less PEG-Mal, no better result was reached. A kinetic investigation of the reaction (Figure 2c) shows that the main grafting reaction is finished after close to 3 min and no change can be observed in the GPC trace after 20 min.

The results of the photoinduced block copolymer formation between PDMAA and PEG-Mal are shown in Figure 3. The results are very similar to the results achieved with PAcManEA. The peak in the GPC trace is clearly shifted to lower retention times indicating a successful block copolymer formation. A small shoulder at higher retention times is visible, indicating remaining PDMAA. Again, remaining PDMAA is observed not because the 1:1 ratio was not reached, as several reactions were conducted and for the reaction with less PDMAA a significant signal of left over PEG-Mal was observed. A kinetic investigation of the reaction (Figure 3c) indicates that the main grafting reaction is finished after close to 30 min and no change can be observed in the GPC trace after 40 min. The shoulder at higher retention times could be explained with a side reaction pathway, which consumes the photo-enol group without leading to a block copolymer, although no such side reaction was observed in the model reaction or stability study.

To evidence that the achieved shift in the GPC trace is due to the formation of a block copolymer, a control reaction was conducted. PAcManEA was exposed to the same reaction conditions as for a block formation, without the addition of the PEG-Mal. The results can be found in the Supporting Information (see Figure S 26). For the control reaction, a shoulder can be observed at lower retention times, which does not match the signal of the PAcManEA-*b*-PEG block copolymer. Instead it approximately matches the result one would expect for a block consisting of two PAcManEA chains, indicating that during the irradiation a very reactive species is formed which can react with the polymer chain. The reactive species is most likely the photo-enol, yet the analytical results cannot rule out if a carbon sulfur bond is cleaved to form radicals. In the presence of PEG-Mal, no such side reaction is observed, as it provides an alternate and rapid reaction path for the reactive o-quinodimethane intermediate; consequently, no GPC traces matching PAcManEA-*b*-PAcManEA or PAcManEA-*b*-PEG-*b*-PAcManEA can be found in the results of the block copolymer formation reactions.

Grafting onto Microspheres. The photo-enol process has been employed to graft polymers and biomolecules spatially controlled onto planar surfaces.[4] The chosen surfaces were flat silicon wafers, which were prefunctionalized with the photo-enol group and the grafted molecules were functionalized with the dienophile maleimide. In contrast to the previously reported study,[4] in the present work the grafting macromolecules are carrying the photo-enol groups, so the substrate has to carry a dienophile on the surface. To evidence the versatility of the photo-enol approach, an interesting but more challenging substrate was chosen: porous polymeric microspheres, based on poly(glycidyl methacrylate) (PGMA). The epoxide groups of the PGMA can be functionalized in many ways,[45] e. g. also with dienes that can undergo (hetero) Diels–Alder reactions,[31] or used directly to graft macromolecules onto the surface of microspheres.[46,47] There exists a multitude of different and interesting macromolecules, such as glycopolymers,[31,48] which have been grafted onto microspheres with various techniques,[24] yet to the best of our knowledge no example of a light-triggered process able to impart spatial resolution.

Microsphere Pre-Functionalization. The functionalization of the PGMA spheres with a maleimide moiety is straightforward. A hydroxyl group attached to a furane protected maleimide undergoes a nucleophilic attack of the epoxide moieties of the microspheres under Lewis acid (BF_3·OEt_2) catalysis at slightly elevated temperatures in a heated shaker. Subsequently, without intermediate purification and in one pot, the maleimide is deprotected via heating to 90 °C, which induces a retro Diels–Alder reaction, thus removing the furane (see Scheme 3). After washing and drying, the functionalized particles were analyzed via scanning electron microscopy (SEM), X-ray photoelectron spectroscopy (XPS), and elemental analysis (EA).

The analysis of the spheres (via SEM, XPS, and EA) shows their successful decoration with maleimide species. The SEM

dx.doi.org/10.1021/ma401242g | Macromolecules 2013, 46, 6858–6872

Scheme 3. Maleimide Functionalization of PGMA Microspheres

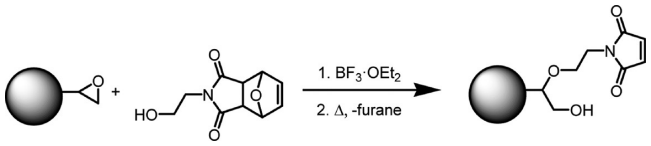

pictures evidence that the spherical shape of the spheres is maintained and the surface morphology of the spheres is not altered (see Figure S 27–S 29). It is always important to check the morphology of the spheres as sometimes even stirring with a magnetic stirring bar can affect their structural integrity.[47] XPS as well as EA demonstrate that compared to the initial PGMA spheres, a clear increase in nitrogen content is detected, thereby evidencing the successful functionalization. XPS shows only noise in the region for nitrogen signals for the untreated spheres and a weak but distinct peak for the maleimide spheres (see Figure 6). The EA shows a nitrogen content of 0.19 wt % for the untreated PGMA microspheres, which probably stems from the radical initiator or stabilizer employed during the synthesis of the particles. After functionalization, the nitrogen content increases to 0.97 wt % (refer to Table S 3 in the Supporting Information for the complete EA results). The increase in the nitrogen content can be correlated to a reaction of approximately one out of five epoxide groups. A functionalization of close to 20% might seem low at first glance, but many of the epoxide groups are buried inside the porous microsphere structure and are therefore much more difficult to access.

Light-Induced Modification of Microparticles. Pre-Test. To evidence the light-triggered modification of the microspheres—which is only due to the photo-enol group reacting with the maleimide moieties—a simple grafting reaction and a control reaction were conducted. The untreated PGMA as well as the maleimide spheres were mixed with DoPATPE in dichloromethane (DCM). DCM was chosen because of its density. As the density of DCM and the microspheres approximately match, the spheres do not sink to the bottom or float on top, yet are evenly distributed within the solution (see Figure S 30). The suspension is subsequently deoxygenated and irradiated for 30 min. Analysis via XPS reveals that only for the maleimide-functionalized spheres sulfur can be detected after the reaction (see Figure 4).

The results of the EA lead to the same conclusion as the ones based on XPS. For the control reaction on nonfunctionalized spheres no sulfur can be found, underpinning the fact that the light-induced Diels–Alder reaction between the maleimide moieties on the particles and the photo-enol leads to the attachment of the DoPATPE. After the photoreaction between DoPATPE and maleimide-functionalized microspheres, the sulfur content increases to 0.40 wt %, implying that 1 g of microspheres contain 4.0 mg of sulfur. The sulfur content can be converted to a loading capacity via the following equation:

$$\mathrm{LC} = \frac{W(\mathrm{S})}{n(\mathrm{S})M(\mathrm{S})} \tag{1}$$

Here LC is the loading capacity (in $\mathrm{mol{\cdot}g^{-1}}$), $W(\mathrm{S})$ is the weight of sulfur per 1 g of microspheres obtained via EA, $n(\mathrm{S})$ is the number of sulfur atoms per grafted molecule (here 3) and $M(\mathrm{S})$ is the molecular weight of sulfur. A loading capacity of 41.6 $\mu\mathrm{mol{\cdot}g^{-1}}$ is reached. Since the relative surface area was measured via inverse size exclusion chromatography to be close to 225.4 $\mathrm{m^2{\cdot}cm^{-3}}$ and the density of the spheres is known as well (1.39 $\mathrm{g{\cdot}cm^{-3}}$) the surface area of the spheres is 1.62×10^{20} $\mathrm{nm^2{\cdot}g^{-1}}$.[31,37] With a known surface area the grafting density can be calculated via

$$\mathrm{GD} = \frac{W(\mathrm{S})N_\mathrm{A}}{n(\mathrm{S})M(\mathrm{S})A} \tag{2}$$

Where GD is the grafting density in chains per unit area; $W(\mathrm{S})$ is the weight of sulfur in 1 g of microspheres obtained via elemental analysis, N_A is the Avogadro's number, $n(\mathrm{S})$ is the number of sulfur atoms per polymer chain, $M(\mathrm{S})$ is the molecular weight of sulfur and A is the surface area of the microspheres. A grafting density of more than 0.15 molecules per $\mathrm{nm^2}$ is reached. The photoinduced reaction leads to a loading capacity in the same order of magnitude as achieved on

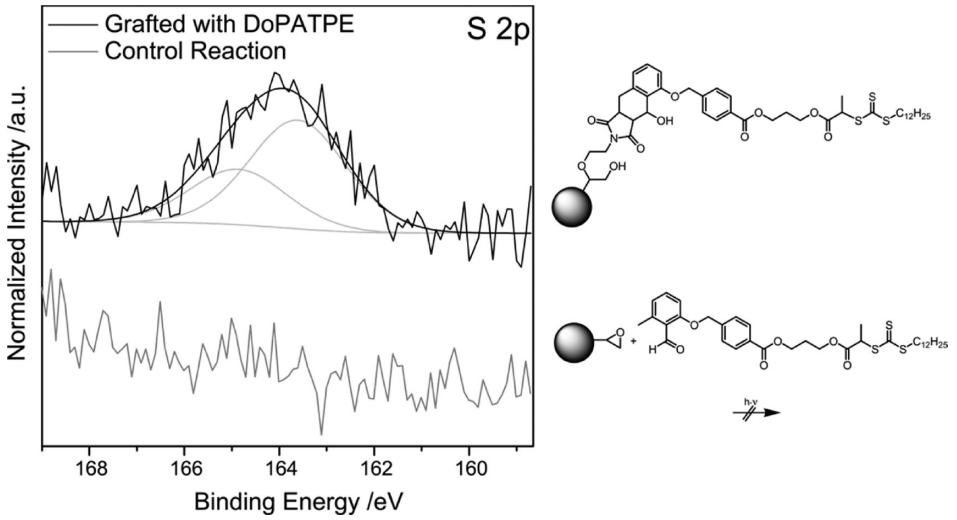

Figure 4. S 2p XP spectra of maleimide-functional microspheres grafted with DoPATPE (top) and the control reaction between PGMA microspheres and DoPATPE (bottom). The presence of sulfur after the successful grafting reaction can only be observed for the maleimide-functionalized spheres.

dx.doi.org/10.1021/ma401242g | *Macromolecules* 2013, 46, 6858–6872

Scheme 4. Light-Induced Grafting Reactions of RAFT-Polymers onto Maleimide-Functionalized Microspheres

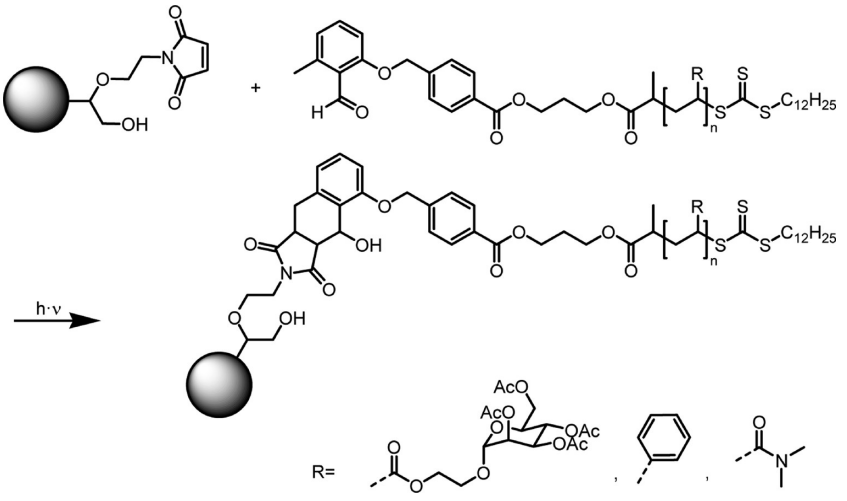

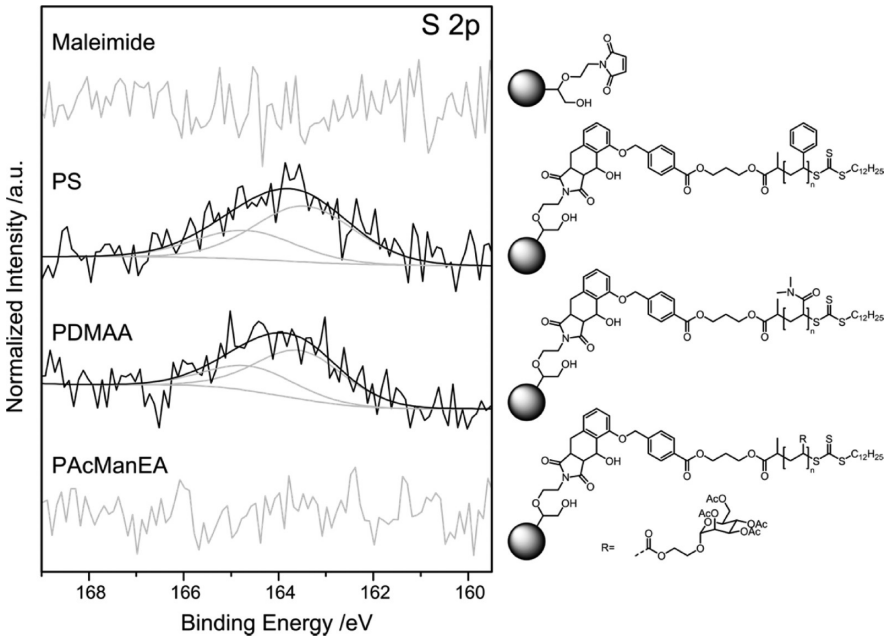

Figure 5. S 2p XP spectra of malemide-functional microspheres (top) and spheres grafted with PS (2nd row), PDMAA (3rd row) and PAcManEA (bottom). The small, yet distinct sulfur peaks for PS- and PDMAA-grafted spheres evidence a successful grafting.

porous PGMA microspheres via a heat-triggered reaction (RAFT-HDA).[31]

Light-Induced Grafting of RAFT-Polymers onto Microparticles. The light-induced modification of microspheres with RAFT-polymers (Scheme 4) proceeds analogous to the test reaction. The spheres and polymers are mixed in DCM (in which the microspheres float, see above and Figure S 30), deoxygenated and irradiated for 30 min. In addition to the analysis via SEM, XPS, and EA, high resolution FT-IR-microscopy can be used in the case of grafted-on PDMAA, as the amide features an additional band in the IR-spectra.

SEM analysis evidences that the spherical shape of the particles as well as the surface morphology is maintained (see Figure S 31−S 39).

Analysis via XPS provides a whole range of information. Sulfur stemming from the RAFT-end-group can be detected for the grafted PS as well as the PDMAA. For grafted PAcManEA, the sulfur cannot be detected (see Figure 5), indicating that probably due to the longer chain length and therefore more steric hindrance a lower grafting density was achieved, which decreases the sulfur content below the detection limit. In the case of PDMAA, the nitrogen signal is also much stronger (see Figure 6), as nitrogen is contained in the repetition unit, and therefore the nitrogen content increases more significantly than the sulfur content. Integration of the entire spectrum yields 0.7 at. % nitrogen for the maleimide spheres and 2.7 at. % for the spheres grafted with PDMAA. Unfortunately, these numbers are not suitable for the calculation of the grafting density, as XPS only analyses the surface of the spheres and especially for minor components it is often insufficiently accurate.

Furthermore, the C 1s peak in the XP spectra can be deconvoluted into several components (see Figure S 40): one at 285.0 eV (C−C, C−H), a second one at 286.5 eV (C−O, C−N), and a third one at 288.9 eV (O−C═O, N−C═O).[49] The ratios of the intensities of the carbon peaks at 285.0 eV (C−C, C−H) and 286.5 eV (C−O, C−N) is depicted in Figure

dx.doi.org/10.1021/ma401242g | *Macromolecules* 2013, 46, 6858−6872

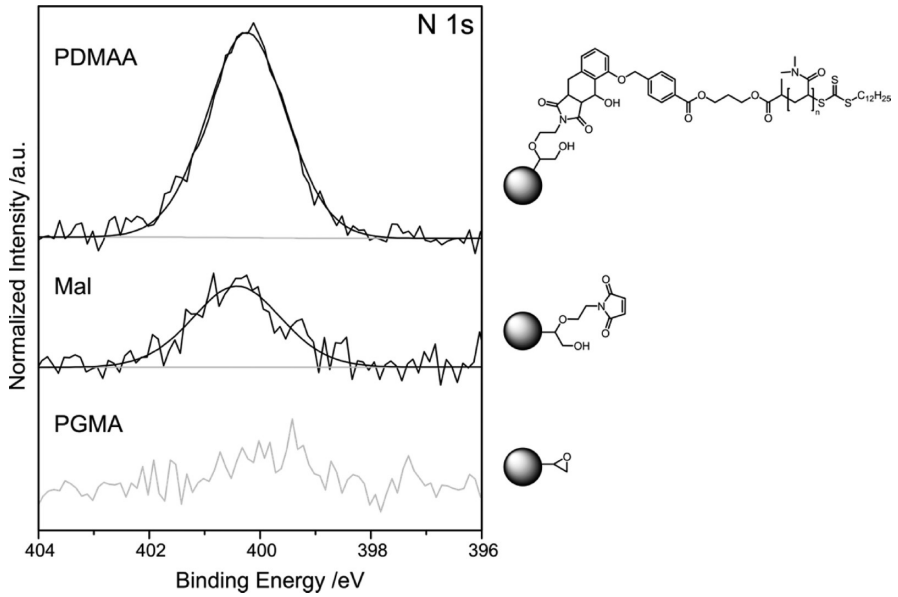

Figure 6. N 1s XP spectra of untreated PGMA microspheres (bottom), maleimide-functionalized spheres (middle) and spheres photografted with PDMAA (top). As expected, no nitrogen peak can be observed for the untreated spheres. After the functionalization with maleimide, a small yet distinct nitrogen peaks is observable. After the grafting of PDMAA, the signal intensity increases. The increase of nitrogen evidences the successful molecular functionalization as well as successful macromolecular grafting.

7 together with additional results from EA which will be discussed in detail below.

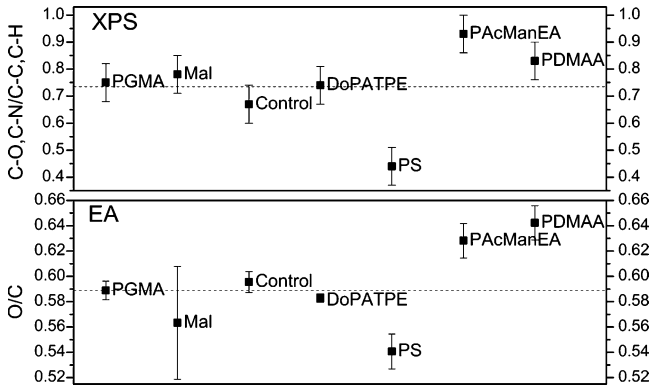

Figure 7. Comparison of the amount of carbon bound to oxygen or nitrogen and carbon bound to carbon or hydrogen based on the deconvolution of the carbon peak in the XP spectra (top) (also see Figure S 40) and the oxygen to carbon ratio determined via EA (bottom). The values are nonchanging for all modifications involving small molecules and show the theoretically expected changes for grafted-on polymers, indicating a successful reaction (for details, see text).

Both analysis techniques show similar results: For the modifications involving small molecules the change in the ratio of carbon bound to carbon and carbon bound to oxygen or nitrogen from the XP spectra and the oxygen to carbon ratio determined via EA is negligible or within the error margins (the error is estimated to be around 10% for XPS and for the EA results the standard deviation was used to calculate an error, see Figure 7). When polystyrene, which only consists of carbon and hydrogen, is grafted onto the microspheres the oxygen to carbon ratios determined via EA and the ratio of carbon bound to oxygen or nitrogen to carbon bound to carbon or hydrogen determined via XPS decreases as expected. In the case of PAcManEA (12 oxygen and 19 carbon atoms, per repetition unit) the O/C ratio rises compared to the PGMA (3 oxygen and 7 carbon atoms) spheres. The same tendency is found in XPS: the signals for C−O, C−N and O−C═O, N−C═O rise in intensity compared to the peak attributed to C−C, C−H (see Figure S 40), as the repeat unit of PAcManEA carries many carbon atoms that are bound to oxygen via single or double bonds. For grafted-on PDMAA, no change in the ratios is expected, yet a small change is visible via XPS. Considering the error in XPS this change is negligible. The strong increase in the O/C ratio determined via EA is associated with traces of residual oxygen or water trapped in the porous structure of the spheres. These results further underpin the successful light-triggered grafting of RAFT-polymers onto microparticles.

Since EA analyses the whole sphere and is very accurate it provides—in contrast to XPS which mainly analyses the surface—quantitative information about the grafting efficiency. Sulfur is also only contained in the chain ends of the polymer, thus—by employing the sulfur value from EA—the loading capacity and grafting density can be determined which is not influenced by any inaccuracies of the chain length analysis of the polymeric chains. For grafted-on PS the sulfur content reaches 0.29 at% and for PDMAA 0.31 at%, respectively. Employing the above-mentioned equations, the sulfur content can be converted to loading capacities of 30.2 μmol·g^{-1} (PS) and 32.2 μmol·g^{-1} (PDMAA) (eq 1) and grafting densities of 0.11 chains per nm^2 (PS) and 0.12 chains per nm^2 (PDMAA) (eq 2). The photoinduced grafting reactions lead to grafting densities which are similar to the grafting densities achieved on porous PGMA microspheres via thermally induced reactions (0.16 chains per nm^2).[31]

For grafted-on PDMAA the nitrogen content reaches 1.39 wt %; for the maleimide-functionalized spheres it reads 0.97 wt %. The increase in nitrogen was not used to determine the grafting density, as this value would be biased by inaccuracies in the chain length value of PDMAA as nitrogen is contained in every repetition unit.

dx.doi.org/10.1021/ma401242g | Macromolecules 2013, 46, 6858−6872

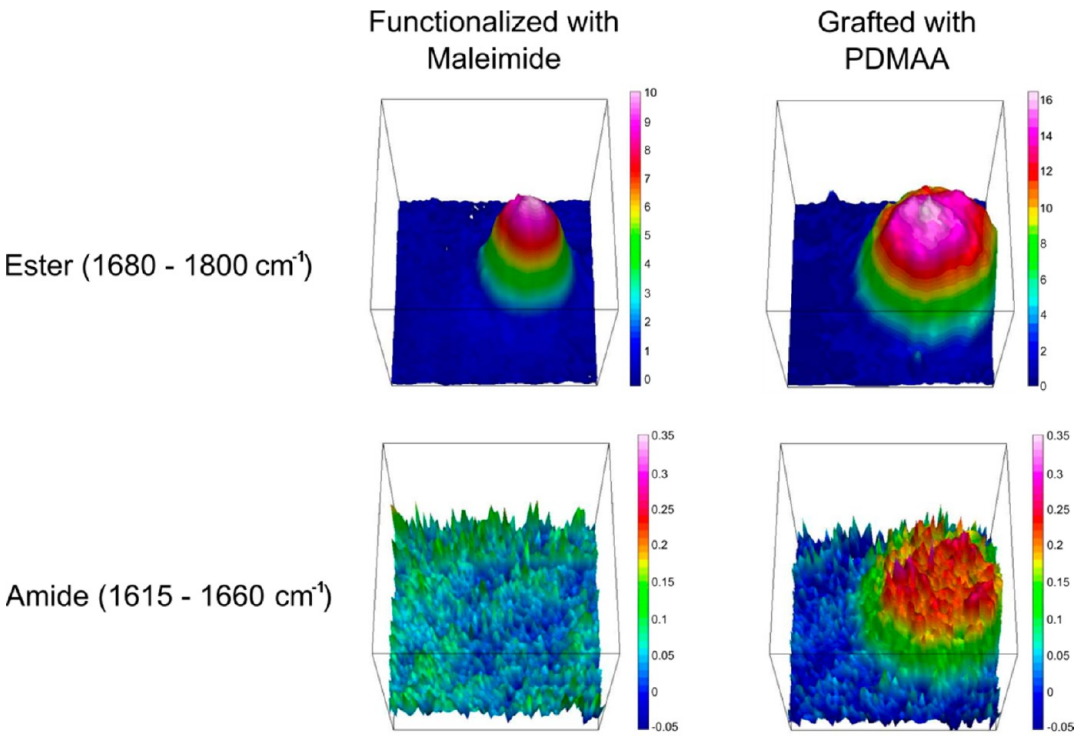

Figure 8. False color high resolution FT-IR microscope images (4 cm^{-1} spectral resolution with a pixel resolution of 0.25 μm^2) of a GMA microsphere functionalized with maleimide and after photografting of PDMAA. The measured area is 32 $\mu m \times 32$ μm. Red color corresponds to a high degree of functionalization. In the top row, the intensity of bands corresponding to the O−C═O stretching vibration is visualized, in the bottom row the N−C═O bands.

No sulfur can be detected for grafted-on PAcManEA, thus no quantitative analysis of the grafting is possible. However, the O/C ratio indicates a successful grafting reaction. A possible reason for the weak sulfur signal may be the length and bulkiness of the PAcManEA chains, which might lead to a higher steric hindrance, therefore a lower grafting density and thus a lower sulfur content are achieved. Yet, the fewer but longer chains lead to a sufficient change in the O/C ratio.

In the case of grafted-on PDMAA amide groups are introduced on the microspheres. Amide vibrations have a band in the IR spectrum which can be distinguished from the ester vibrations.[49] Therefore, high resolution attenuated total reflectance (ATR) FT-IR microscopy can be employed to not only show the successful grafting, yet also its spatial distribution. FT-IR microscopy has been employed before to evidence the successful grafting onto microspheres,[31] and can furthermore even give quantitative information about grafting reactions.[50]

The results of the IR imaging are depicted in Figure 8. As one can see, the mapping of the ester vibration between 1680 and 1800 cm^{-1} depicts the shape of the spheres accurately for the maleimide-functionalized spheres as well as for the ones photografted with PDMAA, as the spheres are based on GMA, which carries an ester group in the repeat unit. In contrast, mapping the amide bond vibration between 1615 and 1660 cm^{-1} gives no signal for the maleimide-functionalized spheres, whereas the spherical shape can clearly be evidenced for the PDMAA grafted particles. Thereby the FT-IR microscopy results not only underpin again the successful grafting, yet also evidence that the grafting is evenly distributed over the whole microsphere.

Synthesis of Janus Particles. The main benefit of employing light-triggered reactions for the grafting of molecules onto surfaces is the possibility of spatial control over the grafting process. When flat surfaces—such as silicon wafers—are the employed substrate, shadow masks, which protect parts of the surface from the irradiation, are employed to generate various patterns.[4,51] Such an approach is not feasible when microparticles are employed. Instead, Janus particles where synthesized via a Pickering emulsion approach. The Pickering effect describes the stabilization of an emulsion via the aggregation of particles at the interface between the two immiscible liquids.[52,53] If the hydrophobic liquid is molten paraffin wax, the particles are trapped on the surface of the wax spheres after they are solidified due to cooling. Thus, only the part of the microparticles that is not covered by the wax can be chemically modified, resulting in Janus particles, which can be isolated after dissolving the wax in a suitable solvent.[28,29]

In the current contribution a Pickering emulsion was established in a round-bottom flask equipped with a magnetic stirring bar. One g of paraffin wax was molten in the presence of the microparticles and water was subsequently added (10 mL). The emulsion was kept at an elevated temperature for 1 h and subsequently allowed to slowly reach ambient temperature. The wax spheres were filtered off, washed intensively and dried. This small and simple approach is sufficient, although the size of the wax droplets is difficult to control and adjust. If a precise control of the wax spheres is necessary, a mechanical stirrer or a commercial reactor with stirring control is recommended.

A Pickering emulsion was conducted with maleimide-functionalized microparticles, resulting in wax spheres of close to 5 mm diameter. These wax spheres were analyzed via SEM, yet the SEM images show a lot of artifacts due to charge build

dx.doi.org/10.1021/ma401242g | *Macromolecules* 2013, 46, 6858−6872

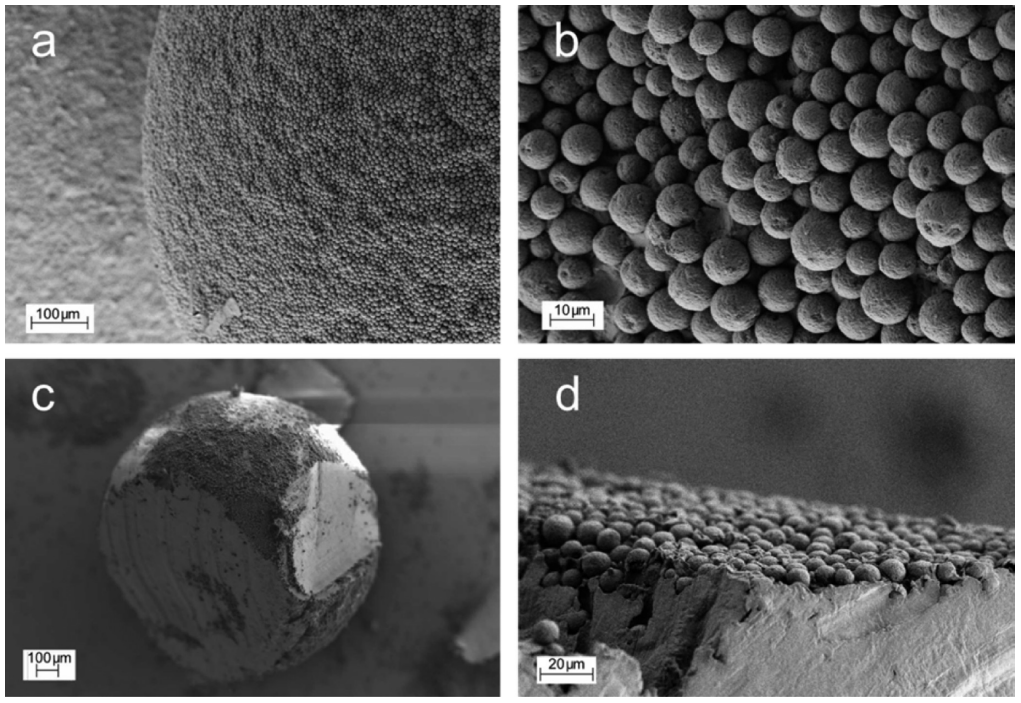

Figure 9. SEM images of wax spheres (diameter approximately 1 mm) covered with PGMA microspheres: (a) overview, (b) close up, (c) a sphere cut with a scalpel, and (d) close up of the surface of the cut sphere. The microspheres are evenly distributed on the surface of the wax sphere, not in the bulk of the wax, and are approximately covered with wax by half.

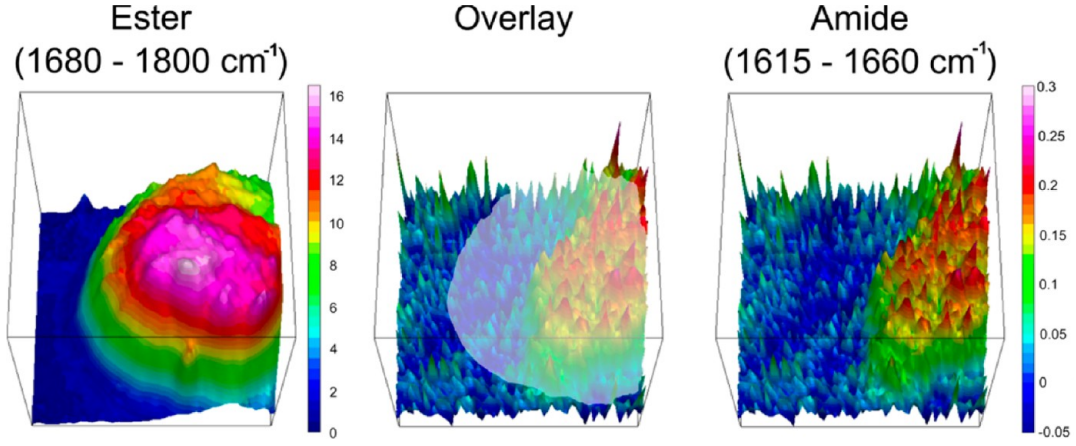

Figure 10. False color high resolution FT-IR microscope images (4 cm^{-1} spectral resolution with a pixel resolution of 0.25 μm^2) of a maleimide-functionalized microsphere after photografting of PDMAA on one-half of the sphere employing a Pickering emulsion approach. The measured area is 32 μm × 32 μm. Red color corresponds to a high degree of functionalization. In the left spectra, the intensity of bands corresponding to the O−C═O stretching vibration is visualized, in the right spectra the N−C═O bands. In the middle, the overlay of the spherical shape taken from the ester band on top of the amide band distribution indicates the Janus-type surface morphology of the particle.

up because of their size (Figure S 41 and S 43). The size of the wax sphere does however not influence the reactivity in photo-triggered grafting reactions.

SEM images of wax spheres covered with untreated PGMA microspheres are depicted in Figure 9 together with images of a wax sphere cut with a scalpel.

The SEM images show that the microspheres are evenly distributed on the surface of the wax sphere which has a diameter of close to 1 mm. The wax covers approximately half of the microspheres. The images of the wax sphere cut with a scalpel reveal that the microspheres can only be found on the surface of the wax and not in the bulk (see Figure 9, parts c and d).

The photoinduced grafting of PDMAA onto the particles embedded in the wax is carried out in analogy to the grafting procedure described above, except that the solvent has to be changed to the more polar methanol (see Scheme 1). Unpolar solvents can dissolve the wax or at least lead to an undesireable swelling of its surface so that the microparticles can leave the wax particle, which would lead to fully grafted spheres without Janus morphology.[29] The reaction mixture was deoxygenated and irradiated for 30 min. Subsequently, the wax was dissolved in chloroform and the now freed microparticles filtered off, washed and dried. The Janus spheres were analyzed via SEM and IR microscopy. The SEM images show that the spherical morphology and porous structure of the particles is maintained

dx.doi.org/10.1021/ma401242g | *Macromolecules* 2013, 46, 6858−6872

and that there is no left over wax adhering to the particles (see Figure S 44–S 46). To illustrate the Janus structure of the photografted spheres, IR imaging microscopy can be employed. A comparison of the distribution of the ester signal and the amide signal clearly evidences that the entire sphere can be imaged via the ester vibration, whereas only half of the sphere is visible if the amide signal is integrated (see Figure 10). The Janus structure is underpinned by an overlay of the spherical shape taken from mapping the ester vibration over the distribution of the amide band. The mapping of the amide band is a little bit noisier as the signal of this band is weaker, since the whole sphere exhibits ester bond, whereas the amide signal stems from a rather short polymeric chain grafted to half of the surface of the spheres. To illustrate this intensity difference, two exemplary IR spectra, one from the left half of the Janus particle—without PDMAA—and one from the right half—with grafted-on PDMAA—are shown in Figure S 47.

These results underpin that the combination of RAFT-polymerization with photoinduced grafting reactions and a Pickering emulsion approach can successfully be employed to synthesize polymeric Janus particles.

CONCLUSIONS

A novel RAFT-agent was synthesized which carries a photoactive group based on ortho-quinodimethane or photo-enol chemistry. The novel RAFT-agent controls the polymerization of a wide range of monomers, such as styrene, dimethylacrylamide and a protected glycomonomer (AcManEA) with dispersities well below 1.2 and high end-group functionalization. The photo-enol group reacts with dieneophiles under mild irradiation at ambient conditions, so that the RAFT-group stays unaltered, and without any catalyst to form block copolymers in a matter of minutes. Furthermore, the RAFT-polymers can also be photografted onto porous polymeric microspheres, after a one-step prefunctionalization with maleimide moieties. The successful grafting is evidenced by SEM, EA, XPS, and high resolution ATR-FT-IR microscopy, which leads to qualitative as well as quantitative information. The grafting densities reaches up to 0.12 molecules per nm^2. To show the benefit of employing a light-triggered grafting reaction the synthesis of Janus particles was conducted, employing a Pickering emulsion approach and illustrated via ATR-FT-IR microscopy.

The current contribution underpins the versatility and robustness of RAFT-polymerization as well as the photo-enol approach. The combination of an easy to use reversible deactivation radical polymerization reaction with a mild light-triggered modular ligation technique opens the door to an entirely new field of opportunities for the synthesis of challenging macromolecule architectures and the modification of surfaces and microparticles.

ASSOCIATED CONTENT

Supporting Information

NMR spectra of the employed molecules and polymers, a schematic drawing of the photoreactor, more analytical data of the model reaction, GPC traces of the employed polymers, ESI-MS spectra of PS and PDMAA, results of the control reaction of PAcManEA, SEM images of the functionalized microspheres, a picture of the microsphere suspension in DCM, the EA data for all samples, XPS comparison of the C 1s peak, a picture and SEM images of the wax spheres decorated with maleimide-functionalized microspheres, and SEM images of the Janus spheres after dissolving of the wax. This material is available free of charge via the Internet at http://pubs.acs.org.

AUTHOR INFORMATION

Corresponding Author

*E-mail: (C.B.-K.) christopher.barner-kowollik@kit.edu.

Author Contributions

All authors have given approval to the final version of the manuscript

Notes

The authors declare no competing financial interest.

ACKNOWLEDGMENTS

M.K. acknowledges funding from the Karlsruhe House of Young Scientists (KHYS) supporting a research stay at the UNSW in Sydney, Australia. C.B.-K. and T.H. acknowledge funding for the current project from the AiF in the context of the ZIM program. We thank the Fraunhofer-Institut für Chemische Technologie ICT in Pfinztal for measuring the elemental analysis. C.B.-K. is additionally grateful for continued support from the Karlsruhe Institute of Technology (KIT) and the Helmholtz association in the context of the BioInterfaces and Science and Technology of Nanosystems program.

REFERENCES

(1) Gruendling, T.; Oehlenschlaeger, K. K.; Frick, E.; Glassner, M.; Schmid, C.; Barner-Kowollik, C. *Macromol. Rapid Commun.* **2011**, *32*, 807–812.

(2) Glassner, M.; Oehlenschlaeger, K. K.; Gruendling, T.; Barner-Kowollik, C. *Macromolecules* **2011**, *44*, 4681–4689.

(3) Winkler, M.; Mueller, J. O.; Oehlenschlaeger, K. K.; Montero de Espinosa, L.; Meier, M. A. R.; Barner-Kowollik, C. *Macromolecules* **2012**, *45*, 5012–5019.

(4) Pauloehrl, T.; Delaittre, G.; Winkler, V.; Welle, A.; Bruns, M.; Börner, H. G.; Greiner, A. M.; Bastmeyer, M.; Barner-Kowollik, C. *Angew. Chem., Int. Ed.* **2012**, *51*, 1071–1074.

(5) Kolb, H. C.; Finn, M. G.; Sharpless, K. B. *Angew. Chem., Int. Ed.* **2001**, *40*, 2004–2021.

(6) Barner-Kowollik, C.; Du Prez, F. E.; Espeel, P.; Hawker, C. J.; Junkers, T.; Schlaad, H.; Van Camp, W. *Angew. Chem., Int. Ed.* **2011**, *50*, 60–62.

(7) Oehlenschlaeger, K. K.; Mueller, J. O.; Heine, N. B.; Glassner, M.; Guimard, N. K.; Delaittre, G.; Schmidt, F. G.; Barner-Kowollik, C. *Angew. Chem., Int. Ed.* **2013**, *52*, 762–766.

(8) Narumi, A.; Fuchise, K.; Kakuchi, R.; Toda, A.; Satoh, T.; Kawaguchi, S.; Sugiyama, K.; Hirao, A.; Kakuchi, T. *Macromol. Rapid Commun.* **2008**, *29*, 1126–1133.

(9) Moad, G.; Rizzardo, E. *Macromolecules* **1995**, *28*, 8722–8728.

(10) Kato, M.; Kamigaito, M.; Sawamoto, M.; Higashimura, T. *Macromolecules* **1995**, *28*, 1721–1723.

(11) Wang, J.-S.; Matyjaszewski, K. *J. Am. Chem. Soc.* **1995**, *117*, 5614–5615.

(12) Chiefari, J.; Chong, Y. K.; Ercole, F.; Krstina, J.; Jeffery, J.; Le, T. P. T.; Mayadunne, R. T. A.; Meijs, G. F.; Moad, C. L.; Moad, G.; Rizzardo, E.; Thang, S. H. *Macromolecules* **1998**, *31*, 5559–5562.

(13) *Handbook of RAFT Polymerization*; Barner-Kowollik, C., Ed.; Wiley-VCH: Weinheim, Germany, 2008.

(14) Nebhani, L.; Barner-Kowollik, C. *Adv. Mater.* **2009**, *21*, 3442–3468.

(15) Gokmen, M. T.; Du Prez, F. E. *Prog. Polym. Sci.* **2012**, *37*, 365–405.

(16) Vaino, A. R.; Janda, K. D. *J. Comb. Chem.* **2000**, *2*, 579–596.

(17) Slater, M.; Snauko, M.; Svec, F.; Fréchet, J. M. J. *Anal. Chem.* **2006**, *78*, 4969–4975.

(18) Li, W.-H.; Stöver, H. D. H. *J. Polym. Sci., Part A: Polym. Chem.* **1998**, *36*, 1543–1551.

(19) Kawaguchi, H. *Prog. Polym. Sci.* **2000**, *25*, 1171−1210.
(20) Barner, L. *Adv. Mater.* **2009**, *21*, 2547−2553.
(21) Zhao, B.; Brittain, W. J. *Prog. Polym. Sci.* **2000**, *25*, 677−710.
(22) Granville, A. M.; Brittain, W. J. In *Polymer Brushes*; Advincula, R. C., Brittain, W. J., Caster, K. C., Rühe, J., Eds.; Wiley-VCH: Weinheim, Germany, 2004; p 33−50.
(23) Nebhani, L.; Sinnwell, S.; Inglis, A. J.; Stenzel, M. H.; Barner-Kowollik, C.; Barner, L. *Macromol. Rapid Commun.* **2008**, *29*, 1431−1437.
(24) Goldmann, A. S.; Barner, L.; Kaupp, M.; Vogt, A. P.; Barner-Kowollik, C. *Prog. Polym. Sci.* **2012**, *37*, 975−984.
(25) Okada, M. *Prog. Polym. Sci.* **2001**, *26*, 67−104.
(26) Gu, W.; Chen, G.; Stenzel, M. H. *J. Polym. Sci., Part A: Polym. Chem.* **2009**, *47*, 5550−5556.
(27) de Gennes, P. G. *Rev. Mod. Phys.* **1992**, *64*, 645−648.
(28) Kaewsaneha, C.; Tangboriboonrat, P.; Polpanich, D.; Eissa, M.; Elaissari, A. *Colloids Surf., A* **2013**, DOI: 10.1016/j.colsurfa.2013.01.004.
(29) Hong, L.; Jiang, S.; Granick, S. *Langmuir* **2006**, *22*, 9495−9499.
(30) Mantovani, G.; Lecolley, F.; Tao, L.; Haddleton, D. M.; Clerx, J.; Cornelissen, J. J. L. M.; Velonia, K. *J. Am. Chem. Soc.* **2005**, *127*, 2966−2973.
(31) Kaupp, M.; Vogt, A. P.; Natterodt, J. C.; Trouillet, V.; Gruendling, T.; Hofe, T.; Barner, L.; Barner-Kowollik, C. *Polym. Chem.* **2012**, *3*, 2605−2614.
(32) Escalé, P.; Ting, S. R. S.; Khoukh, A.; Rubatat, L.; Save, M.; Stenzel, M. H.; Billon, L. *Macromolecules* **2011**, *44*, 5911−5919.
(33) Strazielle, C.; Benoit, H.; Vogl, O. *Eur. Polym. J.* **1978**, *14*, 331−334.
(34) Parry, K. L.; Shard, A. G.; Short, R. D.; White, R.; Whittle, J. D.; Wright, A. *Surf. Interface Anal.* **2006**, *38*, 1497−1504.
(35) Scofield, J. *J. Electron Spectrosc. Relat. Phenom.* **1976**, *8*, 129−137.
(36) Tanuma, S.; Powell, C. J.; Penn, D. R. *Surf. Interface Anal.* **1994**, *21*, 165−176.
(37) Nebhani, L.; Schmiedl, D.; Barner, L.; Barner-Kowollik, C. *Adv. Funct. Mater.* **2010**, *20*, 2010−2020.
(38) Neises, B.; Steglich, W. *Angew. Chem., Int. Ed.* **1978**, *17*, 522−524.
(39) Gruendling, T.; Kaupp, M.; Blinco, J. P.; Barner-Kowollik, C. *Macromolecules* **2011**, *44*, 166−174.
(40) Buback, M.; Junkers, T.; Vana, P. *Macromol. Rapid Commun.* **2005**, *26*, 796−802.
(41) Inglis, A. J.; Sinnwell, S.; Davis, T. P.; Barner-Kowollik, C.; Stenzel, M. H. *Macromolecules* **2008**, *41*, 4120−4126.
(42) Hirschbiel, A. F.; Schmidt, B. V. K. J.; Kaupp, M.; Barner-Kowollik, C. Unpublished Data 2013.
(43) Barner-Kowollik, C. *Macromol. Rapid Commun.* **2009**, *30*, 1625−1631.
(44) Preuss, C. M.; Barner-Kowollik, C. *Macromol. Theory Simul.* **2011**, *20*, 700−708.
(45) Falk, B.; Crivello, J. V. *J. Appl. Polym. Sci.* **2005**, *97*, 1574−1585.
(46) Ma, Z.; Guan, Y.; Liu, X.; Liu, H. *Polym. Adv. Technol.* **2005**, *16*, 554−558.
(47) Vogt, A. P.; Trouillet, V.; Greiner, A. M.; Kaupp, M.; Geckle, U.; Barner, L.; Hofe, T.; Barner-Kowollik, C. *Macromol. Rapid Commun.* **2012**, *33*, 1108−1113.
(48) Pfaff, A.; Barner, L.; Müller, A. H. E.; Granville, A. M. *Eur. Polym. J.* **2011**, *47*, 805−815.
(49) Vogt, A. P.; Tischer, T.; Geckle, U.; Greiner, A. M.; Trouillet, V.; Kaupp, M.; Barner, L.; Hofe, T.; Barner-Kowollik, C. *Macromol. Rapid Commun.* **2013**, *34*, 916−921.
(50) Hansson, S.; Trouillet, V.; Tischer, T.; Goldmann, A. S.; Carlmark, A.; Barner-Kowollik, C.; Malmström, E. *Biomacromolecules* **2012**, *14*, 64−74.
(51) Glassner, M.; Oehlenschlaeger, K. K.; Welle, A.; Bruns, M.; Barner-Kowollik, C. *Chem. Commun.* **2013**, *49*, 633−635.
(52) Pickering, S. U. *J. Chem. Soc., Trans.* **1907**, *91*, 2001−2021.
(53) Binks, B. P. *Curr. Opin. Colloid Interface Sci.* **2002**, *7*, 21−41.